

Sequential Fully Implicit Formulation for Compositional Simulation using Natural Variables

A. Moncorgé^{a,b,*}, H.A. Tchelepi^c, P. Jenny^b

^a*Geoscience Research Center, TOTAL E&P UK, Aberdeen, UK.*

^b*Institute of Fluid Dynamics, ETH Zurich, Zurich, Switzerland.*

^c*Energy Resources Engineering Department, Stanford University, Stanford, California.*

Abstract

The Sequential Fully Implicit (SFI) method was proposed (Jenny et al., JCP 2006), in the context of a Multiscale Finite Volume (MSFV) formulation, to simulate coupled immiscible multiphase fluid flow in porous media. Later, Lee et al. (Comp. Geosci. 2008) extended the SFI formulation to the black-oil model, whereby the gas component is allowed to dissolve in the oil phase. Most recently, the SFI approach was extended to fully compositional isothermal displacements by Moncorgé et al., (JCP 2017). SFI schemes solve the fully coupled system in two steps: (1) Construct and solve the pressure equation (flow problem). (2) Solve the coupled species transport equations for the phase saturations and phase compositions. In SFI, each outer iteration involves this two-step sequence. Experience indicates that complex interphase mass transfer behaviors often lead to large numbers of SFI outer iterations compared with the Fully Implicit (FI) method. Here, we demonstrate that the convergence difficulties are directly related to the treatment of the coupling between the flow and transport problems, and we propose a new SFI variant based on a nonlinear overall-volume balance equation. The first step consists of forming and solving a nonlinear pressure equation, which is a weighted sum of all the component mass conservation equations. A Newton-based scheme is used to iterate out all the pressure dependent nonlinearities in both the accumulation and flux terms of the overall-volume balance equation. The resulting pressure field is used to compute the Darcy phase velocities and the total-velocity. The second step of the new SFI scheme entails introducing the overall-mass density as a degree-of-

*Corresponding author arthur.moncorge@total.com

freedom, and solving the full set of component conservation equations cast in the natural-variables form (i.e., saturations and phase compositions). During the second step, the pressure and the total-velocity fields are fixed. The SFI scheme with a nonlinear pressure extends the SFI approach of Jenny et al. (JCP 2006) to multi-component compositional processes with interphase mass transfer. The proposed compositional SFI approach employs an overall balance for the pressure equation; however, unlike existing volume-balance Sequential Implicit (SI) schemes (Acs et al., SPEJ 1985; Watts, SPEJ 1986; Trangenstein & Bell, SIAM 1989; Pau et al., Comp. Geosci. 2012; Faigle et al., Comp. Meth. App. Mech. Eng. 2014; and Doster et al., CRC 2014), which use overall compositions, this SFI formulation is well suited for the natural variables (saturations and phase compositions). We analyze the ‘splitting errors’ associated with the compositional SFI scheme, and we show how to control these errors in order to converge to the same solution as the Fully Implicit (FI) method. We then demonstrate that the compositional SFI has convergence properties that are very comparable to those of the FI approach. This robust sequential-implicit solution scheme allows for designing numerical methods and linear solvers that are optimized for the sub-problems of flow and transport. The SFI scheme with a nonlinear pressure formulation is well suited for multiscale formulations, and it promises to replace the widely used FI approach for compositional reservoir simulation.

Keywords: nonlinear dynamics, numerical flow simulation, sequential implicit, operator splitting, coupled flow and transport, multiscale methods, flow in porous media, compositional formulation, multiphase flow, multi-component transport, compositional reservoir simulation

Contents

1	Introduction	3
2	Sequential Fully Implicit Scheme for Compositional Flow	6
2.1	Compositional Formulation Based on Extended Natural-Variables	6
2.1.1	Mass conservation equations	6
2.1.2	Constraint equations	8
2.1.3	Thermodynamic volume equation	8
2.1.4	Primary and secondary equations and variables	10
2.2	Sequential Fully Implicit Scheme for Compositional Flow	11

2.2.1	Fully implicit method	11
2.2.2	Nonlinear volume-balance equation	12
2.2.3	Compositional system	14
2.2.4	Comparison with other compositional pressure equations	19
3	Results and Discussion	20
3.1	1D test cases	21
3.1.1	Dead-oil	21
3.1.2	Depletion of a live-oil reservoir	26
3.1.3	Gas injection in a live-oil reservoir	26
3.2	2D test cases	30
3.2.1	2D Case-1: Gas and Water Injection	30
3.2.2	2D Case-2: Gas and Water Injection	36
3.3	3D test cases	38
4	Conclusions	40
5	Nomenclature	45
6	Acknowledgments	46
7	Appendix A: Description of the Models	47
8	Appendix B: SI Metric Conversion Factors	47
9	References	47

1. Introduction

The Sequential Fully Implicit (SFI) method was first proposed to model multiphase fluid flow without mass exchange in the context of the Multiscale Finite Volume (MSFV) method [12]. The SFI approach was later extended to the black-oil formulation (three pseudo components with gas dissolved in the oil phase) [15, 22], and recently for compositional multi-component flow by Hajibeygi & Tchelepi [11], Moncorgé et al. [18, 20] and Møyner et al. [24, 21]. In these previous works, the SFI algorithm consists of solving two different implicit systems in sequence: (1) a pressure equation, and (2) a saturation/composition system. During the solution of the saturation/composition system, the pressure is fixed. For n_c components, a coupled set of $n_c - 1$

component conservation equations is solved in the saturation/composition step. Our objective is to design an SFI scheme with a nonlinear convergence rate that is comparable to that of the Fully Implicit (FI) formulation across the full range of compositional modeling of practical interest. This objective is motivated by several factors. First, multiscale formulations rely on sequential treatment of the flow (near-elliptic) and transport (hyperbolic) problems; thus, in order for multiscale methods to fully replace the existing single-level formulations, the SFI approach must have nonlinear convergence rates that are comparable, or even superior, to Fully Implicit (FI) solution schemes. Second, sequential treatment of flow and transport makes it possible to employ advanced discretization schemes and scalable solution methods to the different equations in the coupled system.

Moncorgé et al. [20] enriched the pressure equation with Fully-Implicit (FI) coupling in regions that experience phase appearance to ensure convergence of the full system to any given tolerance. This approach is efficient as long as the fraction of cells that have both liquid and vapor phases is relatively small. However, as the number of cells that experience phase appearance/disappearance grows, this approach becomes expensive. In Lee et al. [15] and Møyner et al. [22, 24, 21], the conservation equation of one component is removed when solving the saturation/composition system. Hajibeygi & Tchelepi [11] tried to remove the material-balance error by freezing the overall-mass density in the accumulation term and the total-mass flux between the computational cells. Their algorithm is convergent; however, in cases with strong coupling, the scheme needs large numbers of outer iterations. Acs et al. [1], Watts [33], Trangenstein & Bell [30, 31], Dicks [8], Pau et al. [26], Faigle et al. [10] and Doster et al. [9] developed Sequential Implicit (SI) formulations for compositional multi-component displacements. In these SI formulations, extensive degrees-of-freedom (variables), such as the overall number of moles, or mass, of a component divided by the pore volume, are used.

The developers of SI formulations noted that it is not possible to satisfy all the governing nonlinear equations exactly, and that some inconsistencies must be tolerated. The formulations of Acs et al., Watts, Trangenstein & Bell, Dicks, Pau et al., Faigle et al. and Doster et al. consider the pressure equation as a ‘volume balance’ equation; in the second step of solving the transport, they keep the conservation equations of all the components. Upon convergence, the mass conservation equation of each of the components is satisfied subject to the desired tolerance; however, some discrepancies in

the overall-volume balance and the total-velocity persist. Only the overall-volume balance splitting error has been defined in these previous works. Attempts to reduce this volume splitting error have been done in Acs et al., Trangenstein & Bell, Pau et al., Faigle et al. and Doster et al. by using a local relaxation term to keep the error bounded in time or by local smoothing by Dicks. They all result in local changes relaxing the mass balance equations. However, these volume splitting errors are very local and have rarely large effect on the overall flow. On the contrary, the total-velocity splitting error, has never been documented before and has a much larger support. We show that we need to control this second splitting error to recover the fully-implicit solution.

Acs et al., Watts, Trangenstein & Bell, Pau et al., Faigle et al. and Doster et al. employ a linearized ‘volume balance’ equation. Coats [5] proposed an IMPES (IMplicit Pressure EXplicit Saturations) pressure equation built by algebraic manipulations of the usual material balance equations. Møyner et al. [21, 23] use this pressure for their sequential implicit method for compositional flow. The derivatives of the overall compressibility wrt pressure and the derivatives of the partial molar volumes wrt pressure are not accounted for in the linearized ‘volume balance’ equation and the derivatives of the partial molar volumes wrt pressure are not accounted for in the Coats pressure equation. Both equations experience nonlinear convergence difficulties, especially when the coupling between the multiphase flow and the multi-component transport is strong. Here, we propose a nonlinear ‘volume balance’ equation that accounts for all the necessary derivatives wrt pressure. For immiscible and incompressible multiphase flow, the nonlinear pressure equation that we derive here simplifies to the pressure equation of Acs et al., Watts, Trangenstein & Bell, Pau et al., Faigle et al. Doster et al. as well as the pressure equations of Coats and Young [34]. It is also identical to the pressure equation for immiscible multiphase flow of Jenny et al. [12] and to the pressure equation of Lee et al. [15] and Møyner & Lie [22] for the black-oil formulation.

This new SFI scheme with a nonlinear pressure equation can be seen as an adaptation of existing SI methods based on overall compositions to one suited for the natural-variables formulation. The splitting of the coupled system into two nonlinear problems, namely, a nonlinear pressure equation and a nonlinear multi-component transport problem, leads to volume-balance and total-velocity errors. We analyze these ‘splitting errors’, and we show how to control them. We then demonstrate that the parabolic pressure equation

and the hyperbolic transport systems are easier to solve separately using widely available linear solvers compared with the specialized solvers (e.g., CPR-AMG [2]) needed to deal with the full system with mixed parabolic-hyperbolic behaviors.

The paper is organized as follows. First, we introduce a natural-variables formulation, which entails forming a nonlinear volume-balance equation followed by solving the full set of transport equations. Then, we elaborate the details of constructing the volume-balance equation. We also analyze the splitting errors and how to control them. We finally demonstrate the performance of the compositional SFI scheme for very challenging test cases.

2. Sequential Fully Implicit Scheme for Compositional Flow

In this section, we describe the compositional formulation based on natural-variables for both Fully Implicit (FI) and Sequential Fully Implicit (SFI) nonlinear solution algorithms. We present a variant of the natural-variables formulation, whereby the system is augmented by an additional equation and an additional variable. Following that, the new SFI scheme for compositional flow is described.

2.1. Compositional Formulation Based on Extended Natural-Variables

The generalized compositional formulation, which accounts for multi-component, three-phase flow with interphase mass transfer, is the target of this work. We assume that we have n_c components, i.e., n_h hydrocarbon components and the water component, and we employ the natural-variables formulation [4]. The overall density, ρ_t , is used as an additional global variable. The number of unknowns in the case of three-phase flow is $2n_h + 7$. They are: gas-phase pressure, P_g , oil-phase pressure, P_o , water-phase pressure, P_w , total mole density ρ_t , the saturations of each phase, S_g , S_o , S_w , the component mole (mass) fractions in the gas, y_c , and the liquid, x_c . To close the system, $2n_h + 7$ equations are required.

2.1.1. Mass conservation equations

The conservation of a hydrocarbon component, c , and of the water component, w , can be written as:

$$\frac{\partial}{\partial t} [\phi (y_c \rho_g S_g + x_c \rho_o S_o)] + \nabla \cdot [y_c \rho_g u_g + x_c \rho_o u_o] = y_c \rho_g q_g + x_c \rho_o q_o \quad (1)$$

$$\text{and } \frac{\partial}{\partial t} [\phi \rho_w S_w] + \nabla \cdot [\rho_w u_w] = \rho_w q_w, \quad (2)$$

where ϕ is the porosity, ρ_g , ρ_o and ρ_w are the fluid-phase mole densities, and q_g , q_o and q_w source terms. The velocity of each phase $p \in \{g, o, w\}$ is given by Darcy's law:

$$u_p = -\frac{k_{r_p}}{\mu_p} K (\nabla P_p - \bar{\rho}_p g \nabla D) = -\lambda_p K (\nabla P_p - \bar{\rho}_p g \nabla D), \quad (3)$$

where K is the rock permeability, k_{r_p} the relative permeability of each phase, μ_p the phase viscosities, $\lambda_p = \frac{k_{r_p}}{\mu_p}$ the phase mobilities, $\bar{\rho}_p$ the fluid-phase mass densities, g the gravitational acceleration, D the depth. The total-velocity

$$u_t = -\sum_p \lambda_p K (\nabla P_p - \bar{\rho}_p g \nabla D) \quad (4)$$

is the sum of the phase velocities. The phase velocities

$$u_p = \frac{\lambda_p}{\lambda_t} u_t + \sum_q \frac{\lambda_p \lambda_q}{\lambda_t} K [(\nabla P_q - \bar{\rho}_q g \nabla D) - (\nabla P_p - \bar{\rho}_p g \nabla D)] = \frac{\lambda_p}{\lambda_t} u_t + \Psi_p \quad (5)$$

can be expressed as a function of the total-velocity, where $\lambda_t = \sum_p \lambda_p$ is the total-mobility and $\Psi_p = \sum_q \frac{\lambda_p \lambda_q}{\lambda_t} K [(\nabla P_q - \bar{\rho}_q g \nabla D) - (\nabla P_p - \bar{\rho}_p g \nabla D)]$ represents the capillary pressure and gravity contributions for each phase. Writing the phase velocities in terms of the total-velocity (5), and substituting into equations (1) and (2), rewriting the source terms, and adding the total-mole density ρ_t as an additional variable in the accumulation term leads to:

$$\begin{aligned} \frac{\partial}{\partial t} \left[\phi \frac{y_c \rho_g S_g + x_c \rho_o S_o}{\sum_p \rho_p S_p} \rho_t \right] + \nabla \cdot \left[y_c \rho_g \left(\frac{\lambda_g}{\lambda_t} u_t + \Psi_g \right) + x_c \rho_o \left(\frac{\lambda_o}{\lambda_t} u_t + \Psi_o \right) \right] \\ = \left(y_c \rho_g \frac{\lambda_g}{\lambda_t} + x_c \rho_o \frac{\lambda_o}{\lambda_t} \right) q_t \quad (6) \end{aligned}$$

$$\text{and } \frac{\partial}{\partial t} \left[\phi \frac{\rho_w S_w}{\sum_p \rho_p S_p} \rho_t \right] + \nabla \cdot \left[\rho_w \left(\frac{\lambda_w}{\lambda_t} u_t + \Psi_w \right) \right] = \rho_w \frac{\lambda_w}{\lambda_t} q_t, \quad (7)$$

where $q_t = \sum_p q_p$. Equations (6) and (7) are the conservation equations in 'transport form'.

2.1.2. Constraint equations

The $n_h + 5$ constraint equations involve variables in the control-volume (cell) under consideration. We have:

$$\sum_{c=1}^{n_h} y_c = 1, \quad (8)$$

$$\sum_{c=1}^{n_h} x_c = 1 \quad (9)$$

$$\text{and } S_g + S_o + S_w = 1. \quad (10)$$

We also have the capillary-pressure versus saturation relationships:

$$P_{cGO}(S_g) = P_g - P_o \quad (11)$$

$$\text{and } P_{cOW}(S_w) = P_o - P_w, \quad (12)$$

where P_{cGO} and P_{cOW} are the capillary pressures between gas and oil phases and the oil and aqueous phases, respectively. The remaining constraints represent thermodynamic phase equilibrium for each hydrocarbon component (n_h equations). These local equilibrium constraints are applied only when both hydrocarbon phases (oil and gas) are present in the control volume. Existing formulations can be based on black-oil, or K-value correlations [7], as well as the Peng-Robinson [27], Redlich-Kwong [28] and Soave-Redlich-Kwong [29] cubic equations of state (EOS) models. They can all be written as [16]:

$$\hat{f}_{c,g}(P_g, y_1, \dots, y_{n_h}) = \hat{f}_{c,o}(P_g, x_1, \dots, x_{n_h}). \quad (13)$$

2.1.3. Thermodynamic volume equation

The mole-fraction of each phase is denoted $\beta_p(P, z)$ with $p \in \{g, o, w\}$. The overall mole-fraction of a component, $z := (z_\alpha)_{\alpha=c,w}$ can be expressed in terms of the natural variables as:

$$z_c = \frac{y_c \rho_g S_g + x_c \rho_o S_o}{\sum_p \rho_p S_p} \quad (14)$$

$$\text{and } z_w = \frac{\rho_w S_w}{\sum_p \rho_p S_p}. \quad (15)$$

The phase-split algorithm is used to solve the system of $2n_h + 3$ equations and $2n_h + 3$ variables y_c , x_c and β_p with the pressure, P , and the overall

mole-fractions, z , fixed.

$$z_c = y_c \beta_g + x_c \beta_o \quad (16)$$

$$z_w = \beta_w \quad (17)$$

$$\hat{f}_{c,g}(P_g, y_1, \dots, y_{n_h}) = \hat{f}_{c,o}(P_g, x_1, \dots, x_{n_h}) \quad (18)$$

$$\sum_p \beta_p = 1.0 \quad (19)$$

$$\text{and } \sum_c y_c = 1.0. \quad (20)$$

Since $\sum_p \beta_p = 1.0$ and $\sum_{\alpha=c,w} z_\alpha = 1.0$, the last equation is equivalent to $\sum_c x_c = 1.0$. To compute the thermodynamic values of the saturations and the mole-fractions, we first compute the overall mole-fractions with (14) and (15), we then solve the phase-split system to get the thermodynamic values of the mole-fractions y_c and x_c . Finally, we use the β_p to compute the normalized thermodynamic values of the saturations (normalized values needed for the relative permeabilities and the capillary pressures functions):

$$\overline{S}_p^{thermo} = \frac{\frac{\beta_p}{\rho_p}}{\sum_q \frac{\beta_q}{\rho_q}}. \quad (21)$$

The phase-split computations follow the work in [17].

In addition to the $n_c = n_h + 1$ conservation equations and the $n_h + 5$ constraint equations, we employ an additional constraint equation and an additional variable. We choose the total-mole density, ρ_t , as the additional variable for two reasons. First, ρ_t is an intensive variable, but unlike saturation or a mole-fraction, it is not a fraction; second, the phase-split computations are independent of ρ_t . Let us define

$$S_p^{thermo} = \rho_t \frac{\beta_p}{\rho_p} \quad (22)$$

as the ‘thermodynamic saturation’ of phase p . It is the volume of phase p divided by the pore-volume. At convergence, the sum of the thermodynamic volumes of the fluid phases must equal the pore volume.

The usual phase saturation, S_p , is referred to as the ‘flow saturation’. With the definition of the thermodynamic saturations, the following rela-

tionship is always satisfied:

$$\sum_p \rho_p S_p^{thermo} = \sum_p \rho_p \left(\rho_t \frac{\beta_p}{\rho_p} \right) = \rho_t \sum_p \beta_p = \rho_t. \quad (23)$$

The additional constraint equation is the ‘thermodynamic volume equation’, namely,

$$\sum_p S_p^{thermo} = \rho_t \sum_p \frac{\beta_p}{\rho_p} = 1.0. \quad (24)$$

If the thermodynamic volume equation is satisfied, then the thermodynamic saturations and the flow saturations are equal, and the following relationship holds:

$$\rho_t := \sum_p \rho_p S_p^{thermo} = \sum_p \rho_p S_p. \quad (25)$$

2.1.4. Primary and secondary equations and variables

We have a nonlinear system of $2n_h + 7$ equations and $2n_h + 7$ unknowns. The $n_c = n_h + 1$ conservation equations are used as the primary equations. In addition to the ‘thermodynamic volume equation’, we have $n_h + 5$ local constraint equations, which make up the secondary equations. The secondary equations are local constraints and only involve the variables of the control-volume (cell) under consideration. When we linearize the system of equations, the secondary equations are used to eliminate algebraically the $n_h + 5$ variables. After the linear solve that computes the update of the primary variables, the update of the secondary variables are computed from the linearization of the secondary equations.

In our formulation, the gas-phase pressure, P_g , is always a primary variable. The remaining n_h primary variables depend on the phase state of the control volume. For oil-water cells, the primary variables are: S_w and $x_1 \dots x_{n_h-1}$; for gas-water cells, the primary variable set is: S_w and $y_1 \dots y_{n_h-1}$; for three-phase cells, the variables are: S_g , S_w and $y_2 \dots y_{n_h-1}$.

The sum of all the component conservation equations leads to:

$$\frac{\partial}{\partial t} \left[\phi \sum_p \rho_p S_p \right] + \nabla \cdot \left[\sum_p \rho_p u_p \right] = \sum_p \rho_p q_p. \quad (26)$$

Substitution of Eq. (25) into the accumulation term and Eq. (5) in the flux

term leads to

$$\frac{\partial}{\partial t} [\phi \rho_t] + \nabla \cdot \left[\sum_p \rho_p \left(\frac{\lambda_p}{\lambda_t} u_t + \Psi_p \right) \right] = \sum_p \rho_p \frac{\lambda_p}{\lambda_t} q_t. \quad (27)$$

These equations represent the total-mole (mass) conservation equation in the standard form (Eq. (26)) and the transport form (Eq. (27)). We use one of these equations to replace one of the component conservation equations. Here, we replace the water mole (mass) conservation equation with the total-mole (mass) conservation equation. Even though the rock-fluids system is compressible, the total-mole conservation equation has near-elliptic behavior. The component conservation equations, on the other hand, have near-hyperbolic behavior.

In the following matrix notation, "P" refers to the gas-phase pressure, "R" refers to the total mole density variable, "T" to the total-mole conservation equation, and "C" refers to both the n_h primary component variables and the hydrocarbon conservation equations. R_C and R_T are then the residuals of the hydrocarbon conservation equations and the total-mole conservation equation, respectively. A_{CC} , A_{CP} , A_{TC} and A_{TP} are then the derivatives of the hydrocarbon conservation equations versus the primary component variables, the derivatives of the hydrocarbon conservation equations versus the gas-phase pressure, the derivatives of the total-mole conservation equation versus the primary component variables and the derivatives of the total-mole conservation equation versus the gas-phase pressure, respectively.

2.2. Sequential Fully Implicit Scheme for Compositional Flow

We use a finite-volume method with single-point upstream weighting for the spatial discretization and a first-order implicit (backward Euler) scheme for the integration in time.

2.2.1. Fully implicit method

The Fully Implicit (FI) method with the natural-variables formulation [4] uses the usual form of the conservation equations (1) and (26) without the thermodynamic volume equation; that is, the variable ρ_t is not used. Upon convergence, if ρ_t is computed according to equation (24), then we have $S_p^{thermo} = S_p$ for each phase $p \in \{g, o, w\}$. Algorithm 1 describes the FI method, in which ϵ denotes the convergence tolerance.

```

compute  $R_C$  and  $R_T$  from equations (1) and (26)
while  $\max(|R_C|, |R_T|) > \epsilon$  do
  compute  $A_{CC}, A_{CP}, A_{TC}, A_{TP}$  from equations (1) and (26)
  compute  $\begin{pmatrix} \delta C \\ \delta P \end{pmatrix} = - \begin{pmatrix} A_{CC} & A_{CP} \\ A_{TC} & A_{TP} \end{pmatrix}^{-1} \begin{pmatrix} R_C \\ R_T \end{pmatrix}$ 
   $C = C + \delta C$ 
   $P = P + \delta P$ 
  compute phase-split only to detect phase appearance
  recompute  $R_C$  and  $R_T$  from equations (1) and (26)
end

```

Algorithm 1: FI method

2.2.2. Nonlinear volume-balance equation

The temporal discretization of the material balance equations (1) and (2) can be written for $\alpha = c, w$ as:

$$\left[\phi \left(\sum_p \rho_p S_p \right) z_\alpha \right]^{n+1} - \left[\phi \left(\sum_p \rho_p S_p \right) z_\alpha \right]^n = \Delta t \tilde{f}_\alpha^{n+1} \quad (28)$$

The contributions from the fluxes and the wells for a hydrocarbon component c and the water component are:

$$\tilde{f}_c^{n+1} = -\nabla \cdot [y_c \rho_g u_g + x_c \rho_o u_o] + y_c \rho_g q_g + x_c \rho_o q_o \quad (29)$$

$$\text{and } \tilde{f}_w^{n+1} = -\nabla \cdot [\rho_w u_w] + \rho_w q_w \quad (30)$$

The superscripts n and $n + 1$ refer to the previous and current timesteps. The Sequential Fully Implicit (SFI) nonlinear volume-balance equation for immiscible flow [12] was obtained as follows: each mole (mass) conservation equation was multiplied by the inverse of the molar (mass) density of the phase, and then summed together. When the flow is immiscible, the inverse of the molar density of the phase is the molar volume of that phase. The equivalent of the molar volume of each phase for compositional flow is the partial molar volume of each component. We define the partial molar volume of component α as:

$$V_{T_\alpha} = \frac{\partial V_T}{\partial N_\alpha} \quad (31)$$

where V_T is the total fluid volume and N_α is the number of moles of component $\alpha = c, w$. In the case of immiscible multiphase flow, where each

component can exist in only one phase, the following relationships are satisfied:

$$\sum_c y_c V_{T_c} = \frac{1}{\rho_g}, \quad (32)$$

$$\sum_c x_c V_{T_c} = \frac{1}{\rho_o} \quad (33)$$

$$\text{and } V_{T_w} = \frac{1}{\rho_w}. \quad (34)$$

As stated by Watts [33], the partial molar volumes, the overall mole-fractions and the overall specific volume $\frac{1}{\sum_p \rho_p S_p}$ satisfy the following relationship:

$$\sum_{\alpha=c,w} z_\alpha V_{T_\alpha} = \frac{1}{\sum_p \rho_p S_p} \quad (35)$$

In this paper, the pressure equation is obtained as the weighted sum of the nonlinear conservation equations (28); the weights are the partial molar volumes. The result can be written as

$$\begin{aligned} \sum_{\alpha=c,w} V_{T_\alpha}^{n+1} \left[\phi \left(\sum_p \rho_p S_p \right) z_\alpha \right]^{n+1} &= \\ \sum_{\alpha=c,w} V_{T_\alpha}^{n+1} \left[\phi \left(\sum_p \rho_p S_p \right) z_\alpha \right]^n &+ \Delta t \sum_{\alpha=c,w} V_{T_\alpha}^{n+1} \tilde{f}_\alpha^{n+1} \end{aligned} \quad (36)$$

Using relationship (35), it follows that

$$\sum_{\alpha=c,w} V_{T_\alpha}^{n+1} \left[\phi \left(\sum_p \rho_p S_p \right) z_\alpha \right]^{n+1} = \phi^{n+1}, \quad (37)$$

and the new nonlinear pressure equation can be written as:

$$\phi^{n+1} = \sum_{\alpha=c,w} V_{T_\alpha}^{n+1} \left[\phi \left(\sum_p \rho_p S_p \right) z_\alpha \right]^n + \Delta t \sum_{\alpha=c,w} V_{T_\alpha}^{n+1} \tilde{f}_\alpha^{n+1} \quad (38)$$

Equation (38) is the nonlinear overall volume-balance. This equation describes the pressure field that equilibrates the system if the flux terms are

taken as implicit functions of the pressure, but the overall mole-fractions are from the previous composition update. In our sequential-implicit solution strategy, we use the Newton method to iterate out the pressure nonlinearities in the overall-volume balance; thus, the derivatives of the partial molar volumes with respect to pressure are required. During the pressure solution stage, the overall mole-fraction of each component (in the control volume) is kept fixed. The constraint equations (8) to (13) are used to get the derivatives of y_c and x_c with respect to P , and equation (21) is used to get the derivatives of the saturations with respect to P . After each Newton iteration (pressure solution), a phase-split computation is performed for each cell. Then, the saturations and mole-fractions for each phase are reset to their thermodynamic equilibrium values. Recent research show that the cost of the phase-split calculations can be reduced to a small fraction of the total simulation cost [17, 32, 13]. Equation (38) is identical to the pressure equation of the SFI method for the dead-oil (immiscible multiphase flow with no mass transfer), where the phase densities are used for the decoupling. It is also identical to the decoupling used by [15, 22] for the black-oil formulation (i.e., gas component can dissolve in the oil phase).

2.2.3. Compositional system

The second step of the sequential implicit method consists of freezing the pressure and total-velocity fields and advecting the components. For this purpose, we use the transport form of the conservation equations (i.e., Eqs. (6) and (27)).

To deal with the transport, two classes of methods have been proposed. The first class uses variables that represent the full fluid content. This is the case for Acs et al. [1], Watts [33], Trangenstein & Bell [30, 31], Dicks [8], Pau et al. [26], Faigle et al. [10] and Doster et al. [9]. The variables used are: the total number of moles (mass) of each component, or the total number of mole (mass) of each component divided by the pore volume. This is equivalent to updating the variables ξ_c and ξ_w defined as $\xi_c = \phi \frac{(y_c \rho_g S_g + x_c \rho_o S_o)}{\sum_p \rho_p S_p} \rho_t$ and $\xi_w = \phi \frac{\rho_w S_w}{\sum_p \rho_p S_p} \rho_t$ and recomputing all the other variables by phase-split computations.

Since these formulations are based on total-mole (total-mass) variables, it is not possible to employ a natural-variables (i.e., saturations-based) formulation to skip the phase-split computations. In the natural-variables formulation, the local equilibrium constraints Eqs. (13) are solved simultaneously

with the conservation equations (6) and (27) by the Newton method, and the phase-split computations are only used to determine if a fluid phase has appeared. After convergence of the coupled system of component conservation equations, the moles (mass) of each component are conserved; however, the thermodynamic volume equation (24) may not be satisfied exactly. Since this error is local, Acs et al. [1], Watts [33], Pau et al. [26], Faigle et al. [10] and Doster et al. [9] proposed to accept the timestep, but to introduce a local relaxation term in order to keep the error bounded in time. Dicks [8] studied the thermodynamic volume error and introduced a smoothing algorithm that locally perturbs the material balance. Trangenstein & Bell [30, 31] mentioned that the pressure equation is a linearization of the thermodynamic volume error, and that it could be possible to add an outer-loop on the pressure and the compositional system. However, in their applications, they accept the timestep after one outer-loop. No study exists of the convergence rate of the outer iterations.

The second class of methods [12, 15, 11, 22, 20, 24, 21] uses saturations and mole- or mass-fractions. Since the composition variables are only fractions, it is necessary to remove one conservation equation during the solution of the coupled transport. It then means that the pressure equation is not considered a volume-balance, but rather a total-mole or total-mass conservation law. In immiscible situations, with the exception of small time scale transient situations, flow and transport usually can be considered decoupled. But for compositional systems, flow and transport usually cannot be decoupled, and it is thus necessary to perform several outer iterations to reduce to an acceptable tolerance. Recently, this second class of methods has been abandoned, that is, the first class of methods is preferred [19, 23].

Here, we propose to converge the system as in the first class of methods with our new extended natural-variables formulation. The pressure and the total-velocity are frozen. The total mole density is used as an independent variable, and we converge the transport system with the $n_h + 1$ conservation equations (6) and (27). The variables are the n_h primary component variables and the additional total mole density variable ρ_t . The advantage of this formulation - compared with using the number of moles, or mass, per component - is that for the compositional update, we retain the benefits of the natural-variables formulation. Namely, we better control the nonlinearities with the saturations as variables and we compute the phase-split calculations only when a new phase is detected. At convergence, all the components are conserved to the prescribed tolerance; however, the thermo-

dynamic volume equation may not be satisfied. We define the total-velocity error as the difference between the total-velocity based on the latest variables after the compositional update and the total-velocity obtained from the pressure solution and frozen during the compositional update. We show that the total-velocity error, which had not been identified before, is present in the invaded regions, and that it is the primary source of nonlinear convergence problems associated with the splitting scheme. This total-velocity error is particularly important in regions experiencing appearance/disappearance of the gas phase during the timestep. The thermodynamic volume residual is defined as

$$R_{thermo} = \sum_p S_p^{thermo} - 1.0 \quad (39)$$

and the relative total-velocity residual as

$$R_{u_t} = \frac{1}{u_t}(u_t^f - u_t), \quad (40)$$

where u_t^f is the total-velocity, which is kept fixed during the composition update, and u_t is the total-velocity computed by equation (4) with the latest updated variables. Upon solving the nonlinear pressure equation, two strategies are possible. The first strategy consists of continuing with outer iterations until the dimensionless residuals $|R_{thermo}|_\infty$ and $|R_{u_t}|_\infty$ (infinity norm) fall below a tight tolerance. For strongly coupled flow and transport, even a tolerance of 0.01 may take many outer iterations, or no convergence may be achieved at all. This strategy is not practical, as it requires too many iterations in order to be competitive with methods like mSFI [20]. The second strategy consists of relaxing the tolerances of $|R_{thermo}|_\infty$ and $|R_{u_t}|_\infty$ in order to achieve convergence with less outer iterations. Another measure of the total-velocity error is based on the divergence of the total-velocity. The dimensionless divergence of the total-velocity is written as

$$\overline{\nabla \cdot u_t} = \frac{\sum_j (Q_t)^{j,i}}{\max(\frac{(V_P)^i}{\Delta t}, \max_j(|(Q_t)^{j,i}|))} \quad (41)$$

where j are the cells surrounding cell i . $(Q_t)^{j,i}$ are the total volumetric rate from cell j to cell i (positive if entering cell i , negative if leaving cell i), $(V_P)^i$ the pore volume of cell i and Δt the discretized timestep. The divergence of

the total-velocity error is defined by the dimensionless residual

$$R_{\nabla \cdot u_t} = \frac{\sum_j (Q_t^f)^{j,i} - \sum_j (Q_t)^{j,i}}{\max(\frac{(V_P)^i}{\Delta t}, \max_j(|(Q_t^f)^{j,i}|), \max_j(|(Q_t)^{j,i}|))} \quad (42)$$

where $(Q_t^f)^{j,i}$ are the total volumetric rates from cell j to cell i that have been frozen during the composition update.

For challenging test cases, we observe that tolerances of 0.2 for $|R_{thermo}|_\infty$, 0.4 for $|R_{u_t}|_\infty$ and 0.1 for $|R_{\nabla \cdot u_t}|_\infty$ are good enough for strongly coupled flow-transport problems. From this point on, we can accept the timestep with the converged accumulation terms computed with the quantities ξ_c and ξ_w . The accepted volume balance error: $\sum_p (S_p^{thermo} - S_p)$ can be added to the pressure system in order to not propagate this error. However, the volume-balance equation (38) already prevents the propagation of the volume-balance error that potentially exists at time t^n by equilibrating volumes at time t^{n+1} . Adding the volume-balance error does not change the results, but may perturb the solution in some situations. We do not recommend its use.

The algorithm of this second strategy is described in Algorithm 2.

```

while  $\max(|R_C|_\infty, |R_T|_\infty) > \epsilon$  or  $|R_{thermo}|_\infty > \epsilon_{thermo}$  or  $|R_{u_t}|_\infty > \epsilon_{u_t}$ 
  or  $|R_{\nabla \cdot u_t}|_\infty > \epsilon_{\nabla \cdot u_t}$  do
    freeze  $z_{\alpha=c,w}$ 
    while  $|\delta P|_\infty > \epsilon_P$  do
      compute derivative wrt  $P$  and residual of volume-balance
      equation (38) with derivatives of  $y_c$  and  $x_c$  given by
      constraints (8) to (13) and derivatives of  $S_p$  by (21)
      solve and update  $P = P + \delta P$ 
      compute phase-split and set  $y_c$ ,  $x_c$  and  $S_p$  to thermodynamic
      values with (16) to (21)
      recompute residual of volume-balance equation (38)
    end
    unfreeze  $z_{\alpha=c,w}$ 
    compute and freeze total-velocity  $u_t$ 
    while  $\max(|\delta C|_\infty, |\delta \rho_t|_\infty) > \epsilon_C$  do
      compute Jacobian and residual of equations (6) and (27) (all
      conservation equations) wrt variables  $C$  and  $\rho_t$ ; constraints
      equations (8) to (13) are used to convert the derivatives wrt
      secondary variables in function of derivatives wrt primary
      variables  $C$ 
      solve and update  $C = C + \delta C$  and  $\rho_t = \rho_t + \delta \rho_t$ 
      compute phase-split only to detect phase appearance
      compute  $R_C$  and  $R_T$  from equations (6) and (27)
    end
    compute  $R_{thermo}$ ,  $R_{u_t}$  and  $R_{\nabla \cdot u_t}$ 
    unfreeze total-velocity  $u_t$ 
  end
  Exact conservative quantities are  $\xi_c$  and  $\xi_w$ 

```

Algorithm 2: Compositional SFI method

In the case of immiscible multiphase flow with one component per phase, our solution and the solution of Jenny et al. [12] are identical. This is not the case for black-oil formulations, where the solution of Lee et al. [15] and Møyner & Lie [22] is relaxing the material balance of one component.

2.2.4. Comparison with other compositional pressure equations

Similar to the nonlinear volume-balance equation, we use the gas-phase pressure P and the overall mole-fractions z_α for each component $\alpha = c, w$. The overall mole-fractions z_α are fixed, and the constraint equations (8) to (13) are used to get the derivatives of y_c and x_c wrt P . Equation (21) is used to get the derivatives of the saturations with respect to P . Sequential formulations for compositional flows were derived in a semi-implicit context by Acs et al. [1], Watts [33], Trangenstein & Bell [30, 31], Dicks [8], Pau et al. [26], Faigle et al. [10] and Doster et al. [9]. In these previous methods, the pressure equation is derived by linearizing the difference between the sum of the thermodynamic volumes of each phase and the pore volume. The resulting pressure equation accounts for the change of volume of the fluids due to the advection of the compositions. We refer to [33] for the derivation of the ‘linearized volume-balance pressure equation’ that can be written in semi-discretized in time form

$$\left[\frac{d\phi}{dP} + \frac{\phi}{\sum_p \rho_p S_p} \frac{\partial \sum_p \rho_p S_p}{\partial P} \right] (P^{n+1} - P^n) = \Delta t \sum_{\alpha=c,w} V_{T_\alpha} \tilde{f}_\alpha^{n+1}. \quad (43)$$

In a semi-implicit situation, we would first converge

$$\left[\frac{d\phi}{dP} + \frac{\phi}{\sum_p \rho_p S_p} \frac{\partial \sum_p \rho_p S_p}{\partial P} \right]^n (P^{n+1} - P^n) = \Delta t \sum_{\alpha=c,w} V_{T_\alpha}^n \tilde{f}_\alpha^{n+1} \quad (44)$$

and then switch to the nonlinear composition update. In a sequential implicit situation we would converge the equation

$$\left[\frac{d\phi}{dP} + \frac{\phi}{\sum_p \rho_p S_p} \frac{\partial \sum_p \rho_p S_p}{\partial P} \right]^\nu (P^{\nu+1} - P^\nu) = \Delta t \sum_{\alpha=c,w} V_{T_\alpha}^\nu \tilde{f}_\alpha^{\nu+1} \quad (45)$$

until $|P^{\nu+1} - P^\nu|$ is small, where the superscripts ν and $\nu + 1$ denote the old and new pressure iteration levels. Coats [5] built a pressure equation by algebraic manipulations of the usual material balance equations, and Møyner et al. [21, 23] use this pressure for their sequential implicit method for compositional flow. Coats’ pressure equation in a sequential implicit setting is

equivalent to converging the equation

$$\sum_{\alpha=c,w} V_{T_\alpha}^\nu \left[\phi \left(\sum_p \rho_p S_p \right) z_\alpha \right]^{\nu+1} = \sum_{\alpha=c,w} V_{T_\alpha}^\nu \left[\phi \left(\sum_p \rho_p S_p \right) z_\alpha \right]^n + \Delta t \sum_{\alpha=c,w} V_{T_\alpha}^\nu \tilde{f}_\alpha^{\nu+1} \quad (46)$$

until $|P^{\nu+1} - P^\nu|$ is small, where the superscripts ν and $\nu + 1$ denote the old and new pressure iteration levels, and z_α in the left-hand-side term is taken at the latest composition iteration level.

The overall compressibility of the system can dramatically change during the transition from a state with only liquid phases present to a state where a gas phase is present. Moreover, V_{T_α} can be very strong functions of pressure as seen in the relationships (32), (33) and (34). It is then possible to encounter cases where the pressure equations (45) and (46) do not converge. It is then necessary to use both the derivatives of the compressibility and the partial molar volumes. The linearized equation (45) and the nonlinear volume-balance equation (38) are only equivalent for incompressible immiscible systems.. The Coats pressure equation (46) and the nonlinear volume-balance equation (38) are different because V_{T_α} depend on pressure, and the left-hand-side of (46) is only equals to ϕ^{n+1} at convergence. However, when the Coats' pressure equation converges, the solution is the same as the nonlinear volume-balance equation.

3. Results and Discussion

The nonlinear strategies used for the numerical experiments with the FI method, the volume balance system, and the compositional SFI method ensure that the variations of pressure, saturations and mole-fractions over a Newton iteration get damped to respectively 1000.0 Psi, 0.2 and 0.2, and that the saturations and mole-fractions are kept between 0.0 and 1.0. If the value of the total mole density ρ_t after a Newton iteration is negative, it is set to zero, and if the variation of ρ_t over a Newton iteration is larger than the maximum allowed value, i.e., if $|\delta\rho_t|_\infty > \max_p \rho_p$, the value of ρ_t is set to $\rho_t = \sum_p \rho_p S_p$.

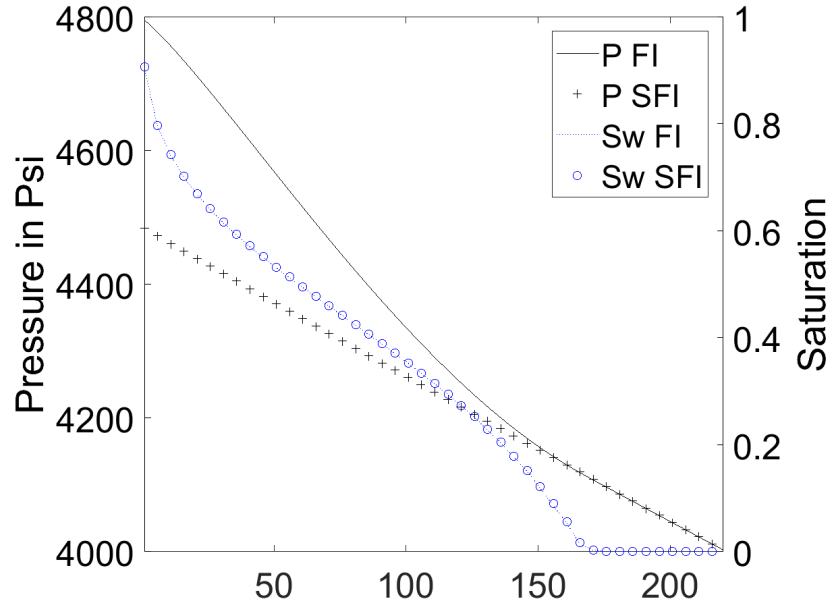
3.1. 1D test cases

In this section we test our compositional SFI algorithm using 1D models; first for dead-oil and then for live-oil fluids.

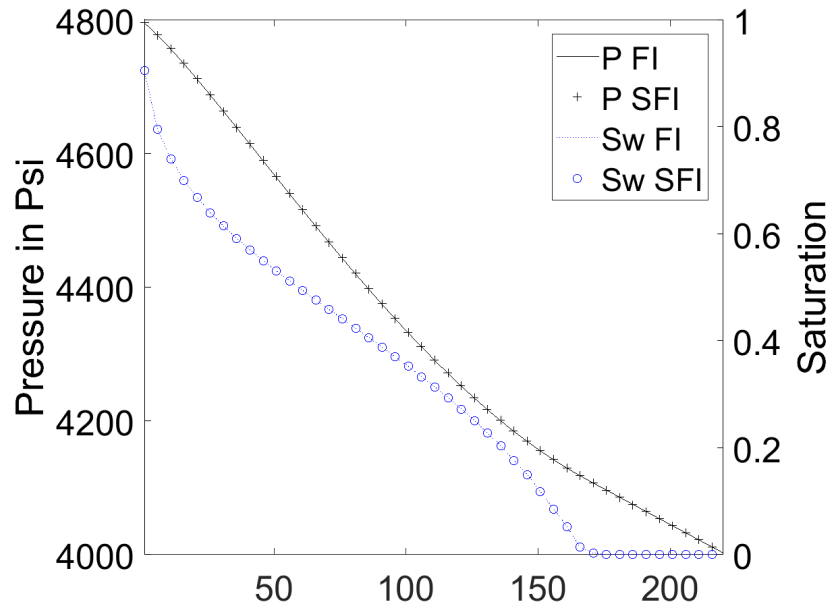
3.1.1. Dead-oil

First, the compositional SFI algorithm is tested for cases with no mass transfer between the fluid phases. We consider injection of water into a reservoir saturated with dead-oil. With a CFL number of 140 [6], the FI method converges in 16 Newton iterations for the first timestep. The SFI method was stopped after one outer iteration of Algorithm 2. The first outer iteration of the SFI method consists of three pressure iterations and 16 compositional iterations. The results are shown in Figure 1a. The saturation fronts obtained with the FI and SFI methods are in very good agreement, but the pressure profiles are quite different. For the SFI method, the material balance equations are satisfied, but the splitting errors $|R_{thermo}|_\infty$, $|R_{u_t}|_\infty$ and $|R_{\nabla \cdot u_t}|_\infty$ are, respectively, $2e-3$, 0.55 and 0.04 . Figure 2 shows the profiles of the three splitting errors. R_{thermo} is very small, R_{u_t} has large values across the 1D domain, and $R_{\nabla \cdot u_t}$ is around 1% except for some localized areas. The total-velocity errors have an impact on the absolute value of the pressure; however, since the system is immiscible and the divergence of the total-velocity is correctly reconstructed, the transport is already correct during the first outer iteration. Two outer SFI iterations (a total of 6 pressure iterations and 18 compositional iterations) are required to fully converge the system with $|R_{thermo}|_\infty$, $|R_{u_t}|_\infty$ and $|R_{\nabla \cdot u_t}|_\infty$ set to $1e-5$, $1e-2$ and $6e-3$, respectively. These results are shown in Figure 1b, and one can observe that the profiles obtained with the FI and SFI methods are identical.

In the second test case, injection of dry-gas into a dead-oil reservoir is considered. The gas, which is less dense, less viscous, and more compressible than the oil phase, is injected with a CFL number of 780. The ratio of the oil to gas mass densities is 735; the ratio of the oil to gas viscosities is 8.1, and the ratio of the gas to oil compressibilities is 0.005. For the first timestep, the FI method converges in 42 Newton iterations. The SFI method was stopped after one outer iteration. The results are shown in Figure 3a. The figure shows that the pressure and saturation profiles obtained with the FI and SFI methods are quite different. The first outer iteration of the SFI method consists of eight pressure iterations and seven compositional iterations ($|R_{thermo}|_\infty$, $|R_{u_t}|_\infty$ and $|R_{\nabla \cdot u_t}|_\infty$ are 0.40, 0.81 and 0.12). Three outer SFI iterations consisting of 18 pressure and 12 compositional iterations



(a) SFI profiles after one outer iteration and converged FI profiles.



(b) Converged SFI and FI profiles.

Figure 1: Water injection: pressure and water saturation profiles versus cell number for the FI and the SFI methods.

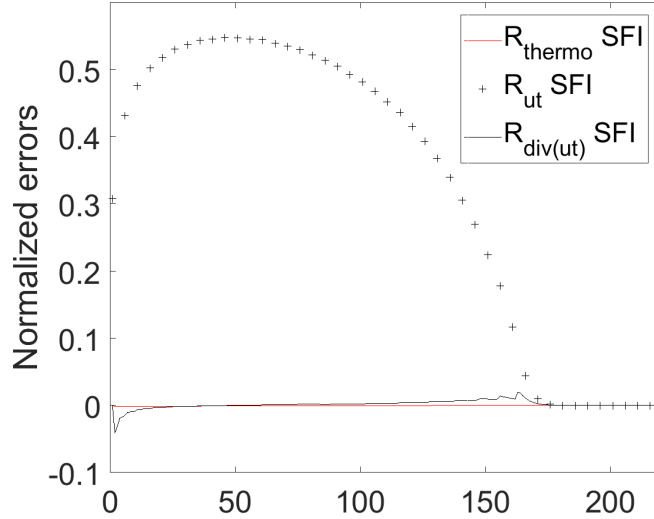
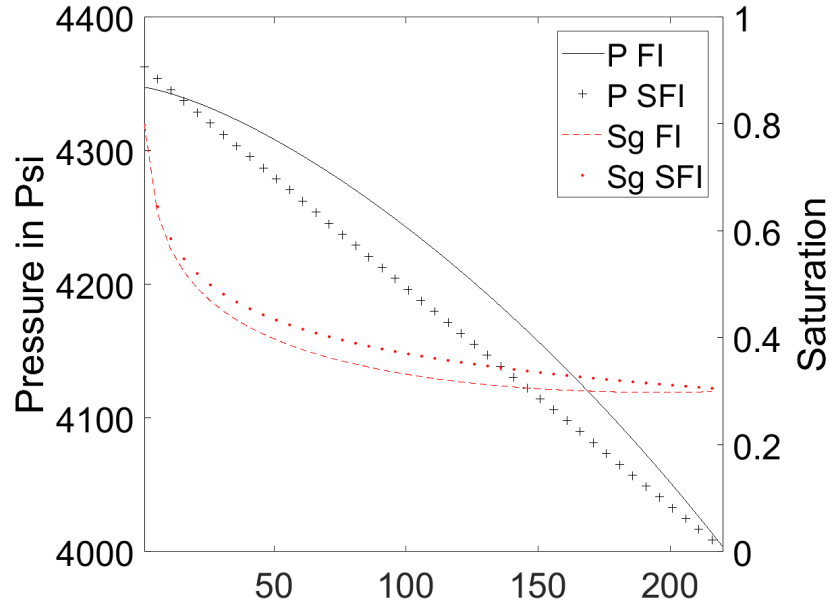


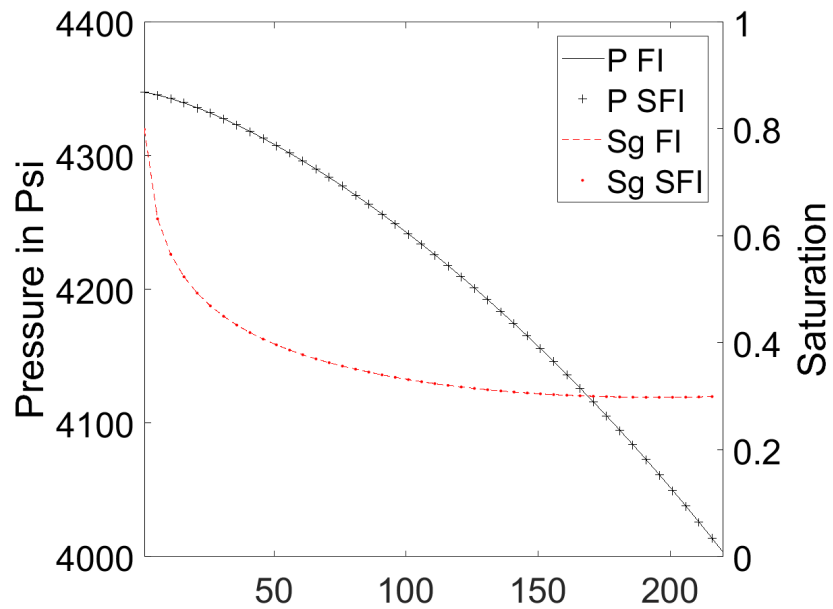
Figure 2: Water injection: thermodynamic volume error R_{thermo} , total-velocity error R_{u_t} and divergence of the total-velocity error $R_{\nabla \cdot u_t}$ for the SFI method after one outer iteration.

are required to converge the SFI method. The results are shown in Figure 3b, and it can be observed that the profiles obtained with the FI and SFI methods are identical.

As a last dead-oil case, gas injection with gravity is considered. Gas is injected into a reservoir initially filled with pure oil, and a CFL number of 65 was applied. The FI method converged in 16 Newton iterations for the first timestep. The SFI method was stopped after one outer iteration. The results are shown in Figure 4a, which depicts pressure and saturation profiles as functions of depth. The pressure and saturation profiles obtained with the FI and the SFI methods are quite different. The first outer iteration of the SFI method consists of 14 pressure iterations and eight compositional iterations ($|R_{thermo}|_{\infty}$, $|R_{u_t}|_{\infty}$ and $|R_{\nabla \cdot u_t}|_{\infty}$ are 0.25, 0.73 and 0.16). Three outer SFI iterations consisting of 27 pressure and 13 compositional iterations are required to converge the SFI method. For this test case with initially pure oil in the reservoir, it is not possible to reach convergence if the usual linearized pressure equation (45) or the Coats pressure equation (46) are employed. The results are shown in Figure 4b, and it can be observed that the profiles obtained with the FI and SFI methods are identical.

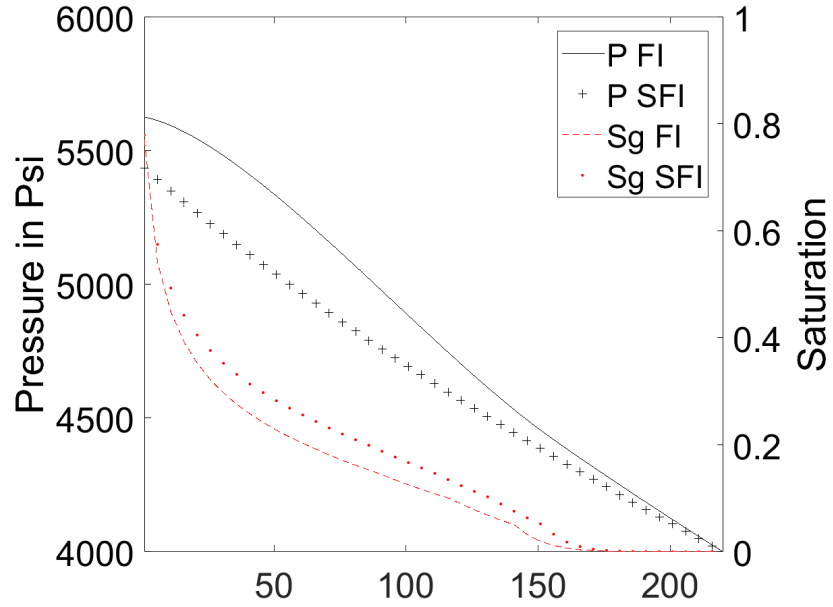


(a) SFI profiles after one outer iteration and converged FI profiles.

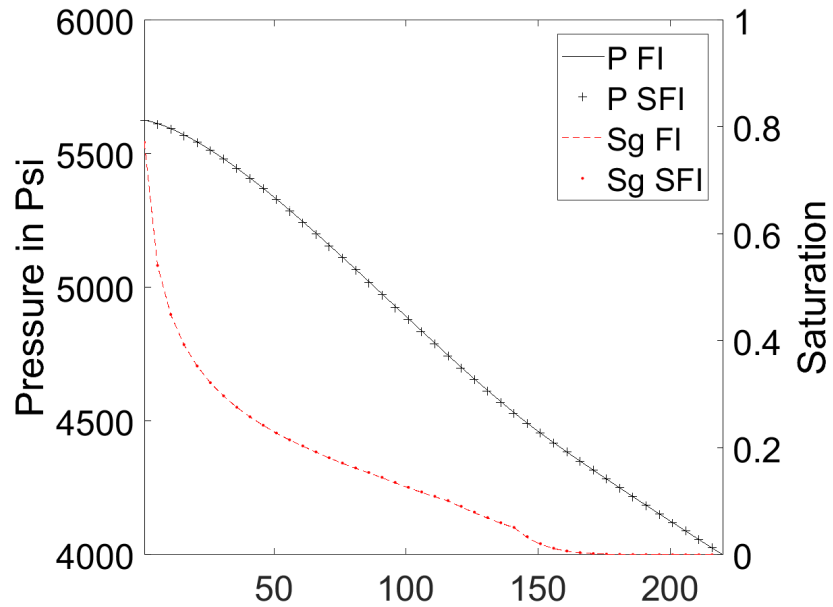


(b) Converged SFI and FI profiles.

Figure 3: Injection of dry-gas: pressure and gas saturation profiles versus cell number for the FI and the SFI methods.



(a) SFI profiles after one outer iteration and converged FI profiles.



(b) Converged SFI and FI profiles.

Figure 4: Injection of dry-gas with gravity: pressure and gas saturation profiles versus cell number for the FI and the SFI methods.

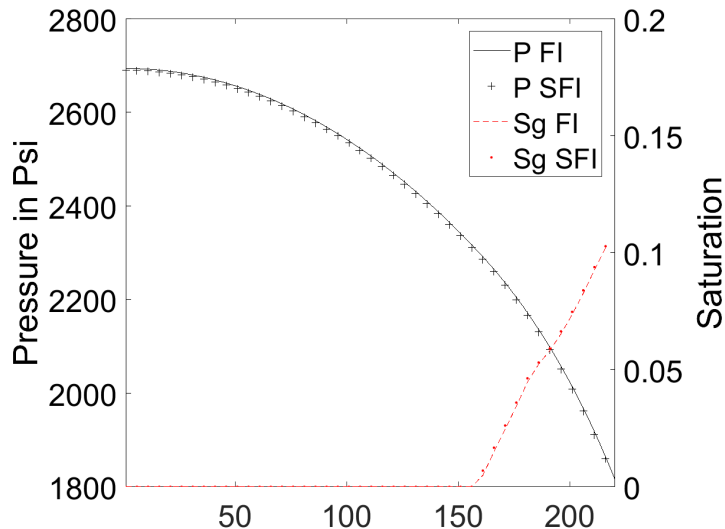


Figure 5: Depletion of live oil: pressure and gas saturation profiles versus cell number for the FI and the SFI methods.

3.1.2. Depletion of a live-oil reservoir

Now that the algorithm is validated for dead-oil cases, we consider a depletion case with the SPE 5 fluid [14]. The reservoir is originally saturated with pure oil, and we drop the pressure at the right-side. In one timestep with a CFL number of 56, gas appears on the right side of the reservoir. The FI method requires seven iterations to converge. One outer iteration of the SFI method consisting of six pressure and three compositional iterations was employed ($|R_{thermo}|_{\infty}$, $|R_{u_t}|_{\infty}$ and $|R_{\nabla \cdot u_t}|_{\infty}$ are 0.36, 0.07 and 0.05). The pressure and gas saturation profiles for the FI and SFI methods are shown in Figure 5. The SFI method converges to the correct solution in one outer iteration even though the thermodynamic volume error of 0.36. However, R_{thermo} is large for a single cell where the gas phases appears. In two outer iterations (consisting of nine pressure and four compositional iterations), $|R_{thermo}|_{\infty}$, $|R_{u_t}|_{\infty}$ and $|R_{\nabla \cdot u_t}|_{\infty}$ decrease to, respectively, 1e-3, 2e-3 and 2e-3.

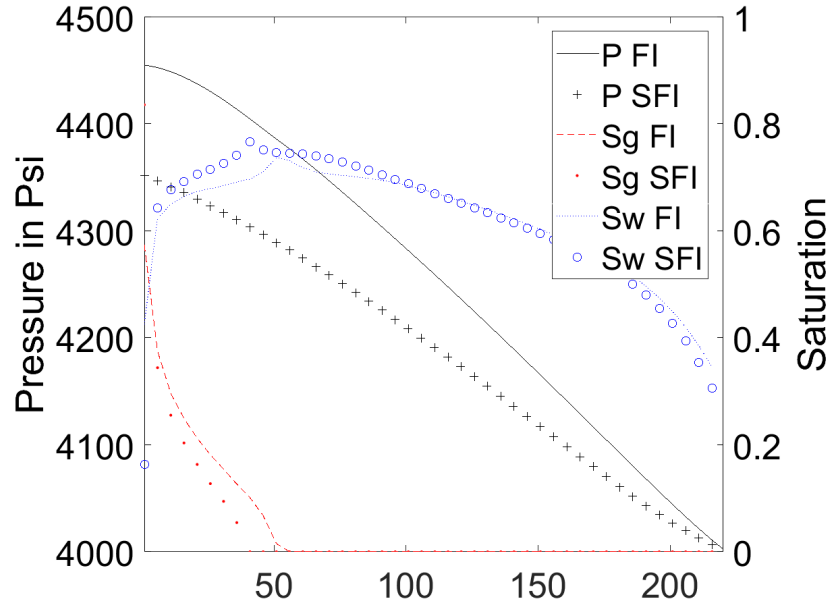
3.1.3. Gas injection in a live-oil reservoir

This test case starts with the initial state shown in Figure 1b. Live-gas is injected into the reservoir. The SPE 5 fluid [14] is used, whereas the light

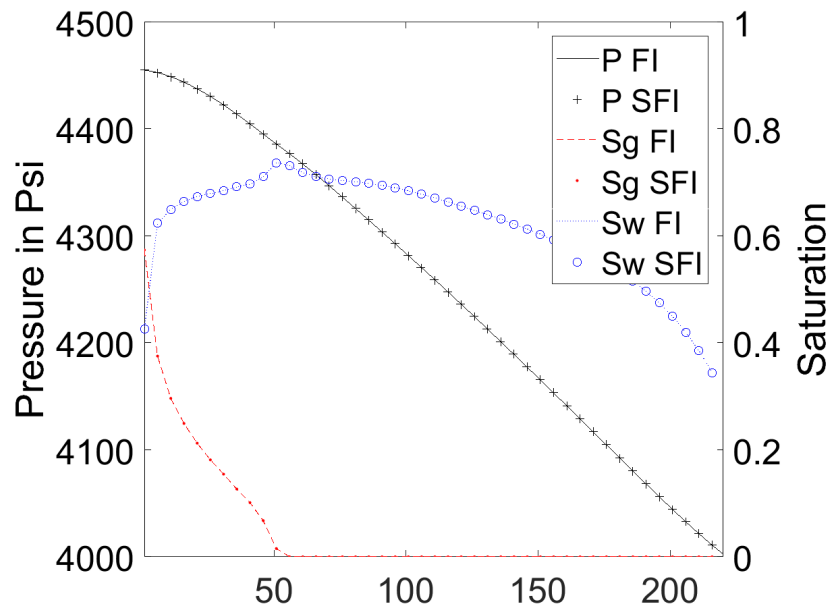
component is injected. Figure 6a shows the pressure and saturation profiles after one timestep with a CFL number of 60 obtained using the FI and the SFI methods. The FI method required 22 iterations to converge. One outer iteration of the SFI method consisting of three pressure and 11 compositional iterations was employed ($|R_{thermo}|_\infty$, $|R_{u_t}|_\infty$ and $|R_{\nabla \cdot u_t}|_\infty$ are 4.95, 0.89 and 0.57). The SFI solutions with one outer iteration are different from the FI results. For complete convergence, 27 iterations (three outer, 9 pressure and 18 compositional iterations) were required; the profiles are shown in Figure 6b.

The next test case describes injection of wet-gas into a reservoir initially filled with live-oil. Figure 7 shows pressure and gas saturation profiles after one timestep with a CFL number of 64 using the SFI method; once after one outer iteration consisting of three pressure and 11 compositional iterations and once after full convergence (requiring in total three outer iterations consisting of 9 pressure and 20 compositional iterations). The FI method requires 37 iterations to converge. After one outer iteration of the SFI method the splitting-errors $|R_{thermo}|_\infty$, $|R_{u_t}|_\infty$ and $|R_{\nabla \cdot u_t}|_\infty$ are 10.2, 0.90 and 0.52, respectively.

The next test case starts with the initial state of Figure 8a and live-gas is injected into the reservoir. Figure 8b shows pressure and gas saturation profiles after one timestep with a CFL number of 76 for the FI method and the SFI method stopped after one outer iteration. The FI method requires 10 iterations to converge. One outer iteration of the SFI method requires three pressure and 9 compositional iterations. The saturation profiles look identical, but the pressure profiles are different. Figure 9 shows the thermodynamic volume error R_{thermo} , the total-velocity error R_{u_t} and the divergence of the total-velocity error $R_{\nabla \cdot u_t}$ profiles for the SFI method. $|R_{thermo}|$ has values up to 8%, $|R_{u_t}|$ has values up to 34% and $|R_{\nabla \cdot u_t}|$ has values up to 14%. On the contrary to the total-velocity error R_{u_t} that has a support on the whole 1D domain, R_{thermo} and $R_{\nabla \cdot u_t}$ have only non-zero values in localized areas. This is an indication that when the compressibility and thermodynamic effects are not too strong we can reconstruct the correct transport in one outer iteration. Table 1 shows the evolution for the SFI method of the thermodynamic volume error, the total-velocity error, the divergence of the total-velocity error as well as the divergence of the total-velocity in function of the number of outer iterations. We observe that the splitting errors $|R_{thermo}|_\infty$, $|R_{u_t}|_\infty$ and $|R_{\nabla \cdot u_t}|_\infty$ decrease with the outer iterations. At some point, the divergence of the total-velocity, $\overline{\nabla \cdot u_t}$, converges to the true value,

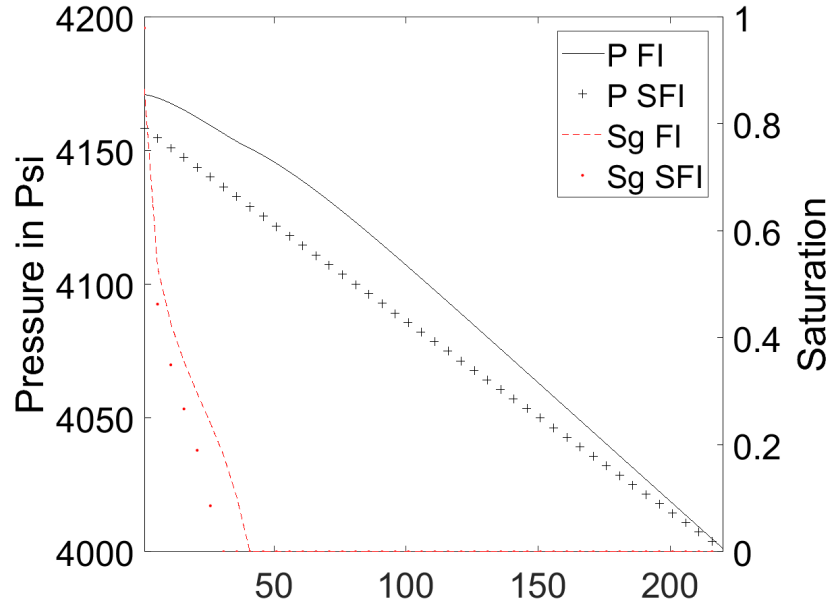


(a) SFI profiles after one outer iteration and converged FI profiles.

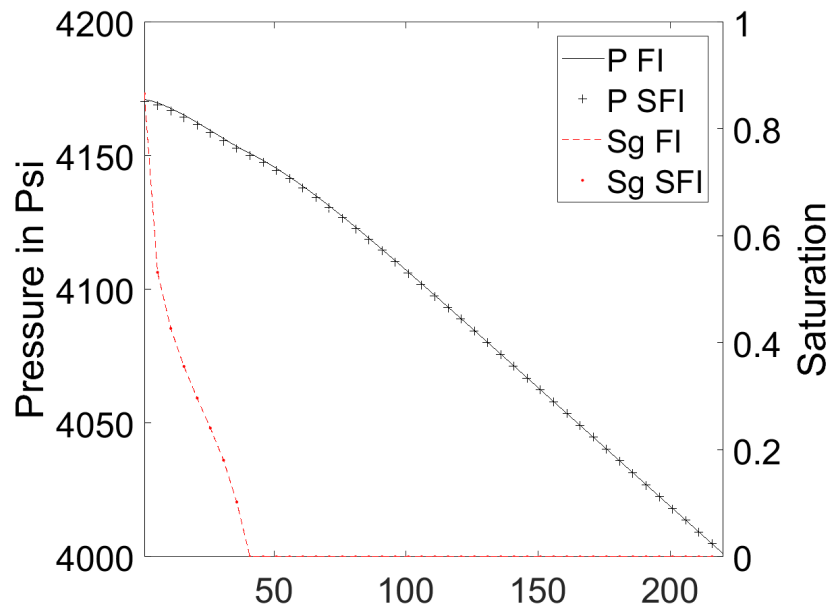


(b) Converged SFI and FI profiles.

Figure 6: Gas injection after water injection: pressure and saturations profiles versus cell number for the FI and the SFI methods.



(a) SFI profiles after one outer iteration and converged FI profiles.



(b) Converged SFI and FI profiles.

Figure 7: Gas injection: pressure and gas saturation profiles versus cell number for the FI and the SFI methods.

Table 1: Gas injection: evolution of the thermodynamic volume error, the total-velocity error, the divergence of the total-velocity error and the divergence of the total-velocity in function of the number of outer iterations.

Outer iterations	P iterations	C iterations	$ R_{thermo} _{\infty}$	$ R_{ut} _{\infty}$	$ R_{\nabla \cdot ut} _{\infty}$	$ \nabla \cdot u_t _{\infty}$
1	3	9	0.08	0.34	0.14	0.14
2	2	2	0.02	0.02	0.02	0.02
3	1	1	1e-3	2e-4	3e-4	3e-3
4	1	1	3e-5	7e-6	6e-6	3e-3
5	1	1	2e-6	1e-6	2e-6	3e-3
6	1	1	2e-8	4e-8	4e-8	3e-3

since the flow is compressible.

Starting from the final state of Figure 7, water is injected for one timestep with a CFL number of 190. Figure 10 shows the pressure and saturations profiles after this timestep. The FI method required 18 iterations to converge. One outer iteration of the SFI method required three pressure and 16 compositional iterations. After this outer iteration, the maximum values of $|R_{thermo}|_{\infty}$, $|R_{ut}|_{\infty}$ and $|R_{\nabla \cdot ut}|_{\infty}$ were 0.34 (in cell 39), 0.89 (in cell 1) and 0.05 (in cell 1), respectively. The pressure and gas-saturation profiles obtained after one iteration with the SFI and FI methods are different. To achieve convergence, SFI scheme required two outer iterations consisting of a total of 6 pressure and 18 compositional iterations.

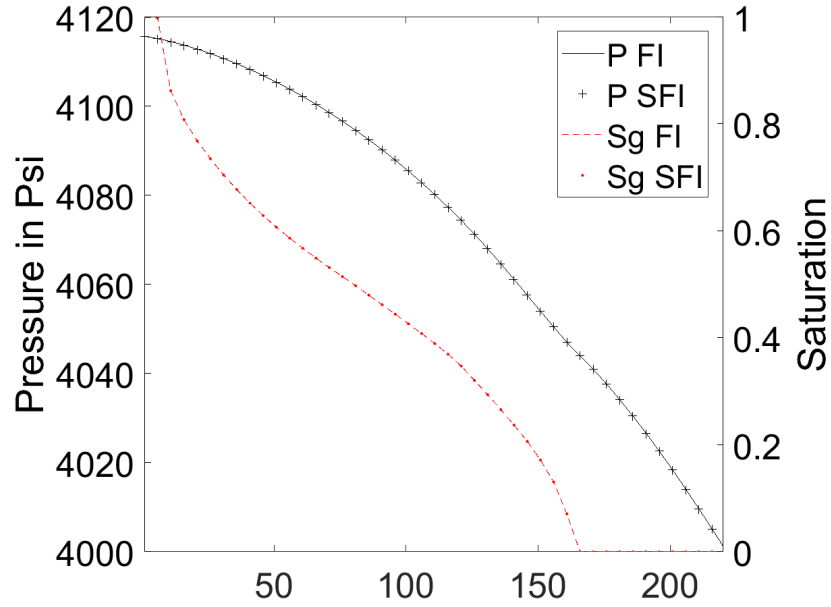
Similar test cases have been simulated with the "system 1" fluid from [35] and the decane/CO₂/methane fluid from [24], and the same observations apply.

3.2. 2D test cases

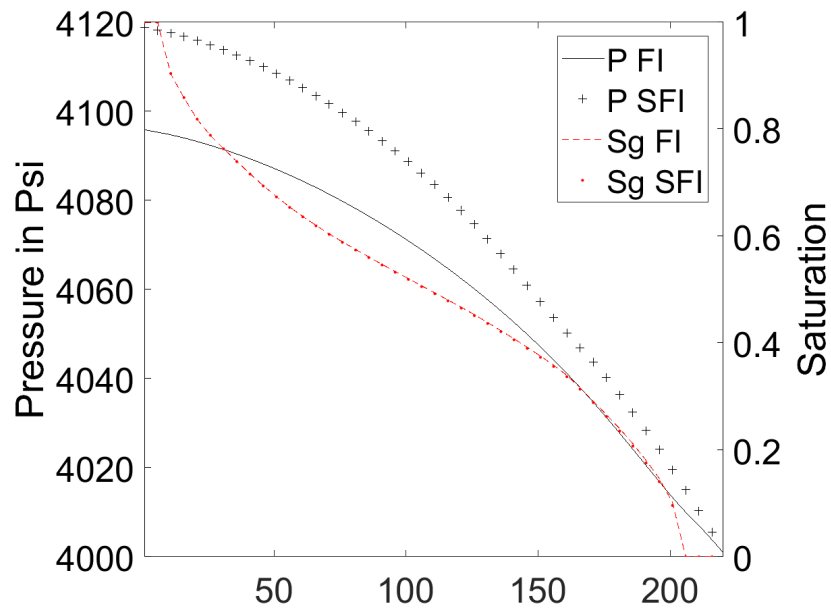
In this section, we present 2D test cases with gas and water injection.

3.2.1. 2D Case-1: Gas and Water Injection

The first test case is from Moncorgé et al. [20]. The light component is injected into multi-component oil at the lower-left corner of the model; the producer, for which the bottom-hole pressure (BHP) is set to 4000 Psi, is located at the upper-right corner of the model. See figure 11a. We study the behaviors for one particular timestep. Figure 11 shows the solution of the SFI method after one outer iteration. The mass balance equations are converged, but the residuals R_{thermo} and R_{ut} are 'relaxed'. The CFL numbers for explicit treatment of saturation (CFL_S) and compositions (CFL_X) [6] are 33 and 224 for the timestep, respectively. The FI method converges in 6 iterations. For the SFI method, we summarize in table 2 the evolution of



(a) Initial SFI and FI profiles.



(b) SFI profiles after one outer iteration and converged FI profiles for a timestep with a CFL number of 76.

Figure 8: Gas injection: pressure and gas saturation profiles versus cell number for the FI and the SFI methods.

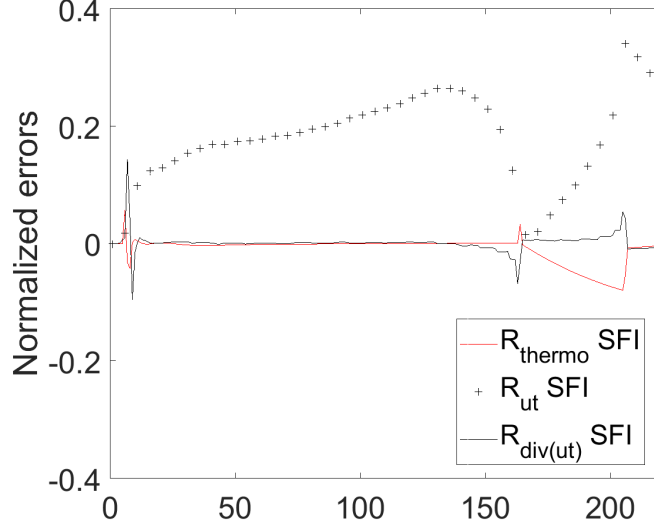


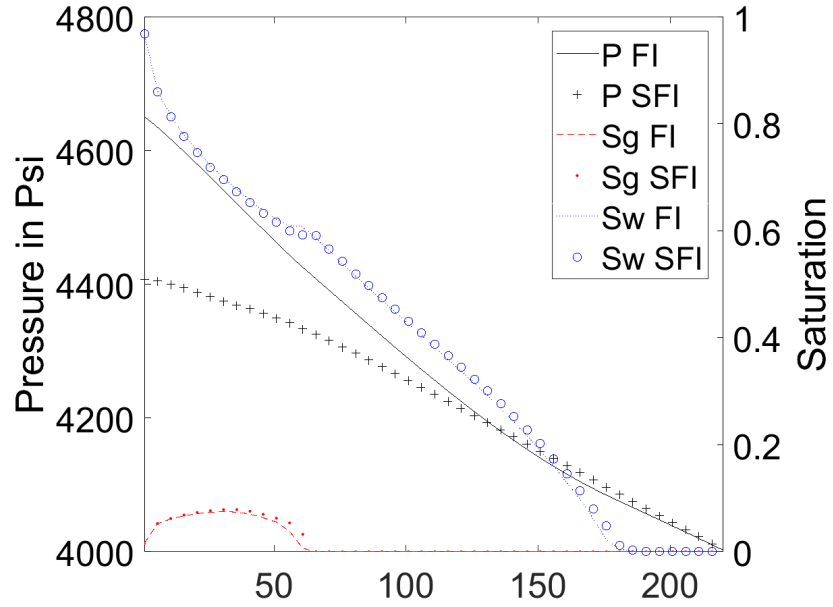
Figure 9: Gas injection: thermodynamic volume error R_{thermo} , total-velocity error R_{u_t} and divergence of the total-velocity error $R_{\nabla \cdot u_t}$ for the SFI method after one outer iteration.

the errors in the thermodynamic volume, total-velocity, and divergence of the total-velocity, as functions of the number of outer iterations. We observe that the splitting errors decrease with the outer iterations. Since the flow is compressible, the divergence of the total-velocity $\overline{\nabla \cdot u_t}$ converges to the correct nonzero value.

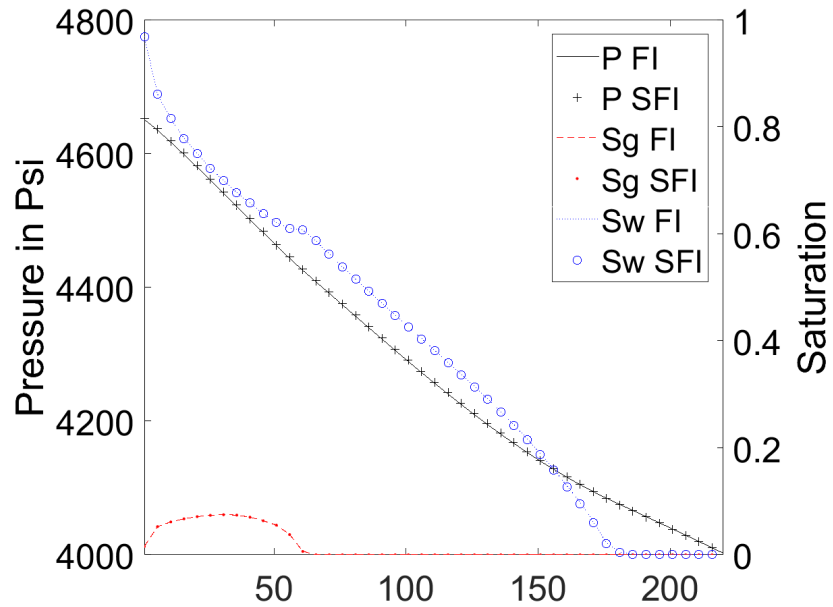
Table 2: Evolution of the thermodynamic volume error, the total-velocity error, the divergence of the total-velocity error and the divergence of the total-velocity as functions of the number of outer iterations for 2D Case-1.

Outer iterations	P iterations	C iterations	$ R_{thermo} _{\infty}$	$ R_{u_t} _{\infty}$	$ R_{\nabla \cdot u_t} _{\infty}$	$ \overline{\nabla \cdot u_t} _{\infty}$
1	2	6	0.07	0.29	0.44	0.44
2	2	3	9e-3	7e-2	0.12	0.18
3	2	1	1e-3	7e-3	9e-3	8e-2
4	1	1	9e-5	1e-3	1e-3	8e-2
5	1	1	6e-6	1e-4	1e-4	8e-2
6	1	1	6e-7	1e-5	1e-5	8e-2

After one outer iteration with two pressure and six compositional solves, we observe highly localized errors at the front between the gas and the oil phases in the thermodynamic volume equation with values that amount up to 7%. The cells with errors of more than 1% for the volume are plotted in



(a) SFI profiles after one outer iteration and converged FI profiles.



(b) Converged SFI and FI profiles.

Figure 10: Water injection: pressure and saturations profiles versus cell number for the FI and the SFI methods.

Figure 11b. Total-velocity errors as large as 29% are observed, and they have a large support as seen in Figure 11c. The cells with errors of more than 5% in the total-velocity are plotted in Figure 11d. Figure 11e shows that errors greater than 5% in the total-velocity divergence are localized. Nevertheless, the largest error is about 44%. For this timestep, we required three outer iterations (a total of six pressure and 10 compositional solves) to converge to the FI solution.

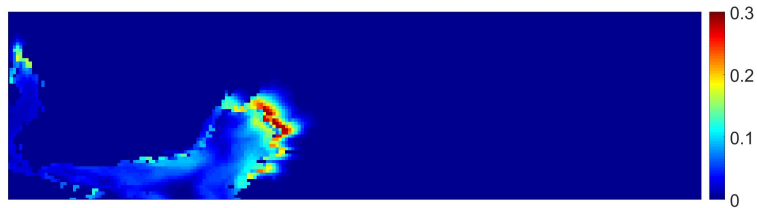
We now study the behaviors for the full simulation. The first period involves injection of the light-component at a rate of six MSCF/Day; the second period entails water injection at a rate of four STB/Day, and the third period involves light-component injection at a rate of six MSCF/Day. This injection strategy leads to complex behaviors with gas fronts chased by water fronts that force the gas to dissolve back into the oil phase. FI requires 399 and SFI 401 timesteps to reach convergence. Figures 12a, 12b and 12c show the gas saturation profiles at the end of each of the three periods. For the first period, the average CFL numbers for the explicit treatment of saturation (CFL_S) and for the explicit treatment of compositions (CFL_X) are 40 and 71, respectively, and the corresponding maximum values are 204 and 228. For the second period, the average values of CFL_S and CFL_X are 39 and 15, respectively, and their maximum values are 500 and 136. For the third period, the average values of CFL_S and CFL_X are 182 and 191, respectively, and the maximum values are 635 and 490. Figure 13 shows the cumulative number of Newton iterations for the FI method and the cumulative number of pressure and composition iterations for the SFI method, as well as the percentage of gas in the model for both the FI and SFI methods. For this test case, the SFI method requires 26% more pressure iterations and 55% more composition iterations than the FI method Newton iterations. The percentage of gas is exactly the same for both models. Figure 14 shows the cumulative number of CPR(AMG,ILU0)-FGMRES iterations required by the FI method and by the pressure solve of the SFI method and the cumulative number of ILU0-GMRES iterations required by the SFI method for the compositional system. Both the full system of the FI method and the pressure systems of the SFI method require around 5 CPR iterations to converge, but the compositional systems of the SFI method only require 2.2 ILU0-GMRES iterations to converge. As a result, for this test case the SFI method takes 33% more linear pressure iterations than the FI method, but only 65% of the FI linear composition iterations. This test case is quite challenging for SFI methods, as the coupling between flow and transport is



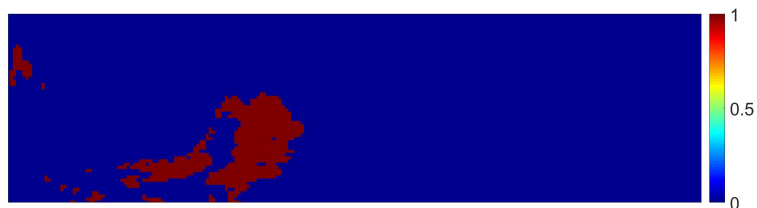
(a) S_g .



(b) Volume error above 1%. Error ranges from -7% to +7%.



(c) Total-velocity error reaches up to 30%.

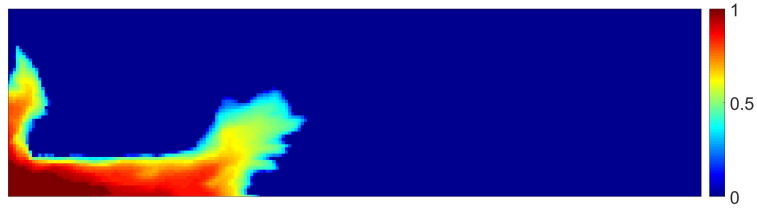


(d) Velocity error exceeding 5%.

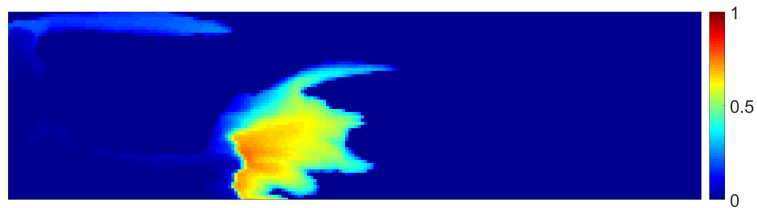


(e) Divergence of velocity error exceeding 5%. Error ranges from -39% to +44%.

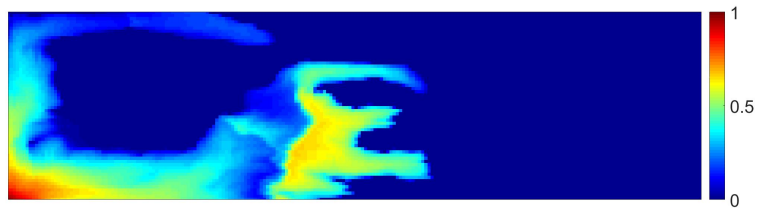
Figure 11: Maps for 2D Case-1 after application of one outer iteration of the sequential algorithm.



(a) After gas injection at the end of the first period.



(b) After water injection at the end of the second period.



(c) After gas injection at the end of the third period.

Figure 12: Gas saturation for 2D Case-1.

strong.

3.2.2. 2D Case-2: Gas and Water Injection

The second test case is challenging for the FI method, but easier for the SFI method. Water is injected at the top-left corner at a rate of four STB/Day and gas at the bottom-left corner at a rate of one MSCF/Day. Production occurs at the top-right and bottom-right corners, where the BHP is set to 4000 Psi. To increase the velocity of the water phase, the porosity in the 20 top layers (out of 60 layers) is reduced by a factor of 100. Note that such contrasts are realistic and represent low porosity corridors. Both the FI and SFI methods require 19 timesteps to converge. Figures 15a and 15b show the water and gas saturation maps at the end of the simulation. A large part of the reservoir has been flooded by water and experiences very fast veloci-

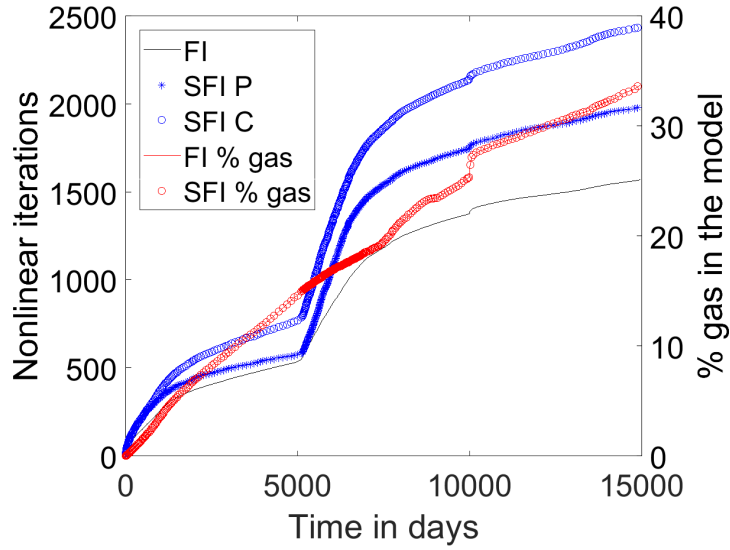


Figure 13: Cumulative Newton iterations for the FI method and cumulative pressure and composition iterations for the SFI method for 2D Case-1. The percentage of gas in the model for the FI and SFI methods is also shown.

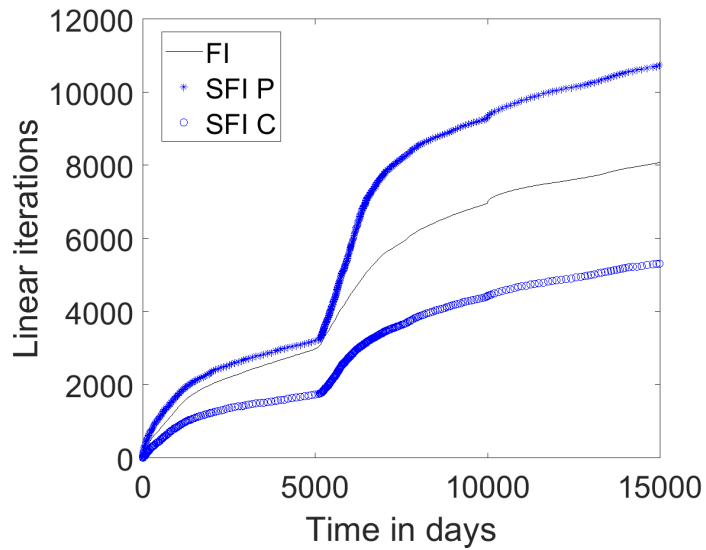
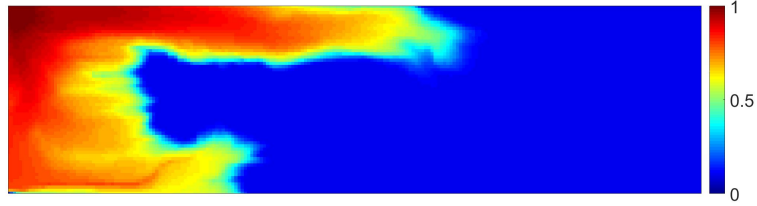


Figure 14: Cumulative CPR iterations for the systems of the FI method and the pressure of the SFI method and cumulative ILU0-GMRES iterations for the composition systems of the SFI method for 2D Case-1.

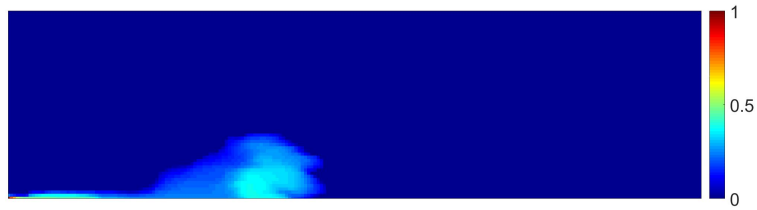
ties; gas is only present in the lower part of the reservoir. While there is no gas-phase in the reservoir initially, at the end of the simulation almost 8% of the cells have gas. The average CFL number per timestep is 480 and the corresponding maximum value is 1140. Figure 16 shows the cumulative number of Newton iterations for the FI method and the cumulative number of pressure and composition iterations for the SFI method as well as the percentage of gas in the model for both the FI and SFI methods. For this case, the SFI method requires 36% fewer pressure iterations and 17% more composition iterations than the FI method Newton iterations. The percentage of gas for the models is exactly the same. Figure 17, shows the cumulative number of CPR(AMG,ILU0)-FGMRES iterations for the FI method and the pressure solves of the SFI method and the cumulative number of ILU0-GMRES iterations for the compositional system of the SFI method. The full system of the FI method requires in average around 8 CPR iterations to converge, while the pressure systems of the SFI method requires around 6 CPR iterations to converge. The compositional systems of the SFI method requires in average 5.3 ILU0-GMRES iterations to converge. As a result, the SFI method for this test case takes 49% of the linear pressure iterations and 78% of the linear composition iterations of the FI method. The strong oil-water flow is challenging for the FI method and very well handled by the SFI method, and the mild compositional effects are handled well by both methods. This is a configuration that is closer to real reservoir simulation scenarios.

3.3. 3D test cases

The 3D model here represents an anticlinal formation. The fluid is modeled as a two-component compositional black-oil formulation. There are four water injectors and six producers. Figure 18 shows the model and the gas saturation at the end of the simulation. Figures 19 and 20 show the injection and production profiles for each phase as well as the average reservoir pressure. We observe that the FI and SFI produce exactly the same results. The FI method converges in 304 timesteps and the SFI method in 361 timesteps. Figure 21 shows the cumulative Newton iterations for the FI method, the cumulative pressure and composition iterations for the SFI method as well as the percentage of gas in the model for both the FI and SFI methods. We see that the percentage of gas in the model changes quite rapidly, and that both methods capture exactly the same physics. These rapid changes are due to the complexity of the medium with strong contrasts between the geological facies. The SFI method requires 20% fewer pressure iterations than the



(a) Water saturation at the end of the simulation.



(b) Gas saturation at the end of the simulation.

Figure 15: Saturation maps for 2D Case-2.

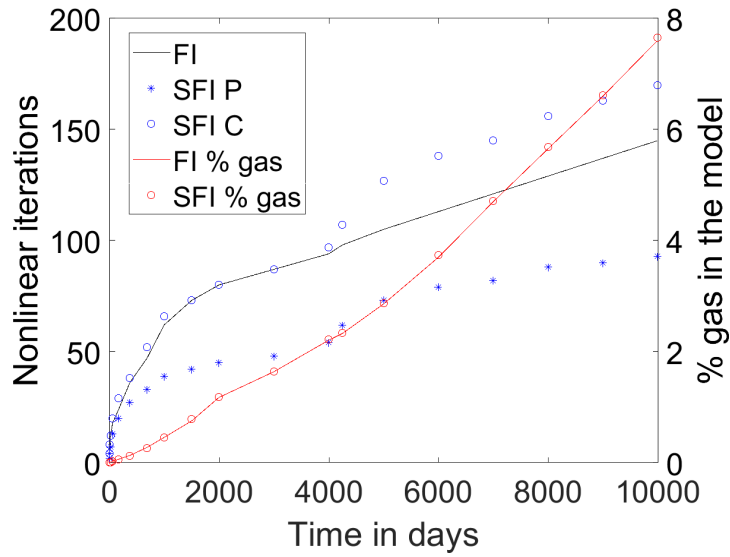


Figure 16: Cumulative Newton iterations for the FI method and cumulative pressure and composition iterations for the SFI method for 2D Case-2. The percentage of gas in the model for the FI and SFI methods is also shown.

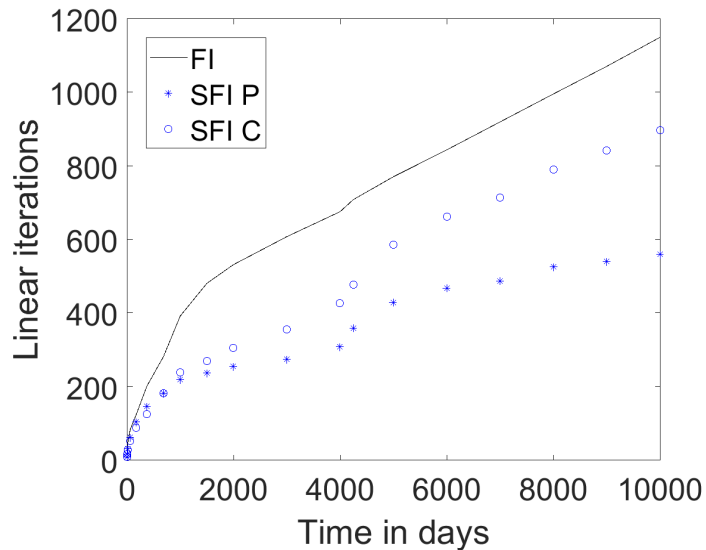


Figure 17: Cumulative CPR iterations for the systems of the FI method and the pressure of the SFI method and cumulative ILU0-GMRES iterations for the composition system of the SFI method for 2D Case-2.

FI method requires Newton iterations and 15% more composition iterations than the FI method requires Newton iterations. Figure 22, shows the cumulative number of CPR(AMG,ILU0)-FGMRES iterations for the FI method and the pressure solves of the SFI method and the cumulative number of ILU0-GMRES iterations for the compositional system of the SFI method. The CPR(AMG,ILU0)-FGMRES system of the FI method requires in average 4.2 iterations, while the pressure system of the SFI method requires in average 3.1 linear iterations and the composition system of the SFI method requires in average 2 linear iterations per system. As a result, the number of linear iterations from the pressure systems of the SFI method amount to 58% of the number of CPR iterations for the coupled system of the FI method, and the number of linear iterations from the composition systems of the SFI method amount to 55% of the number of CPR iterations for the coupled system of the FI method.

4. Conclusions

We proposed a new compositional Sequential Fully Implicit (SFI) solution scheme with a nonlinear pressure equation for compositional flow simulation.

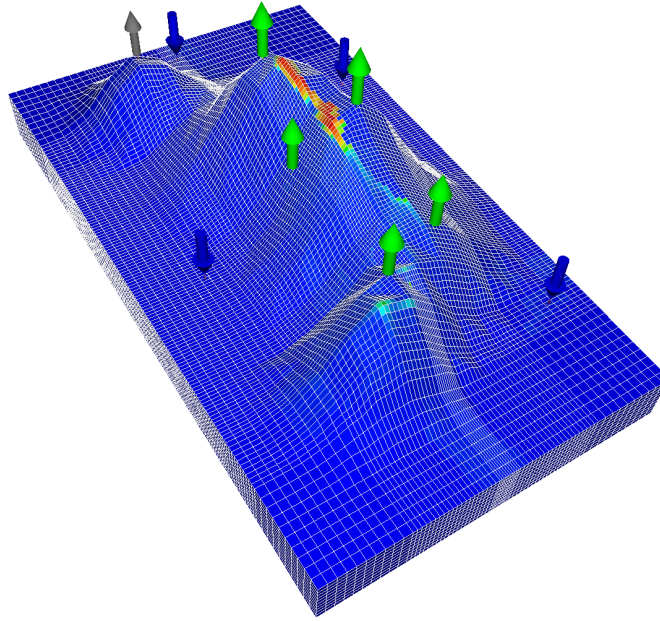


Figure 18: Gas saturation map for the anticlinal model. The water injectors are the blue arrows and the producers are the green arrows. Plotted with ResInsight [25].

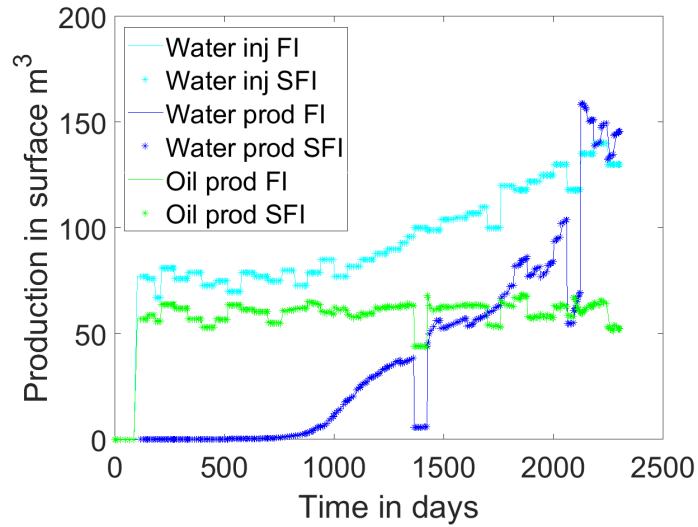


Figure 19: Liquid rates (water injection/production and oil production) profiles for the FI and SFI methods for the anticlinal model.

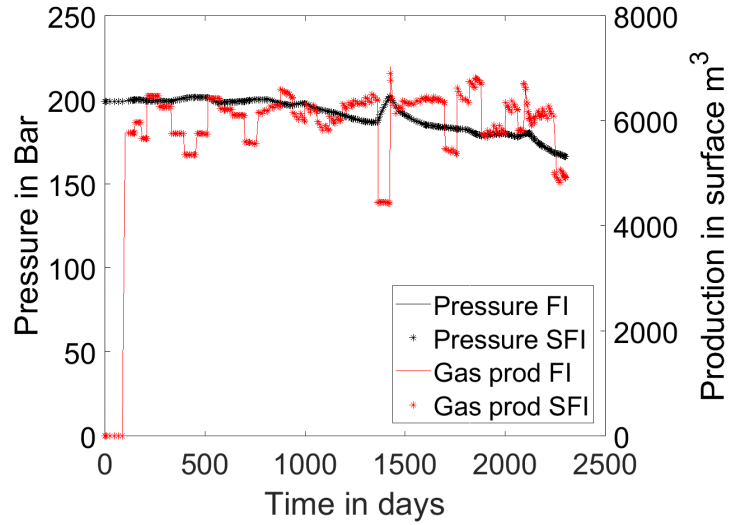


Figure 20: Average reservoir pressure and gas production rate profiles for the FI and SFI methods for the anticlinal model.

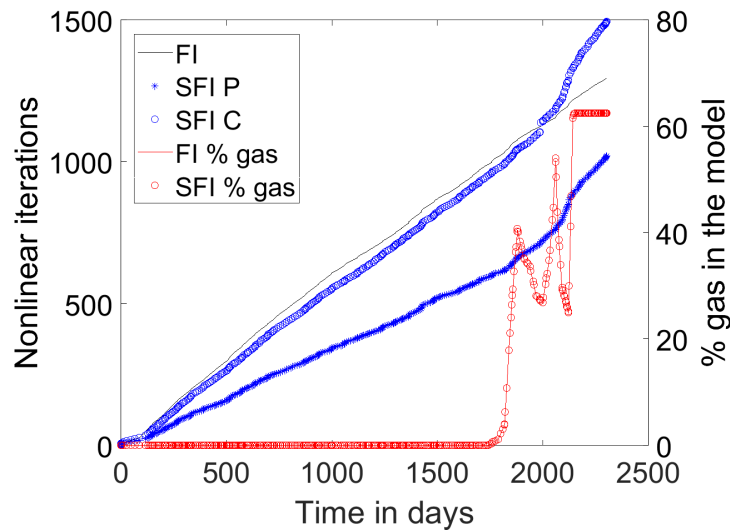


Figure 21: Cumulative Newton iterations for the FI method and cumulative pressure and composition iterations for the SFI method for the anticlinal model. The percentage of gas in the model for FI and SFI methods are also shown.

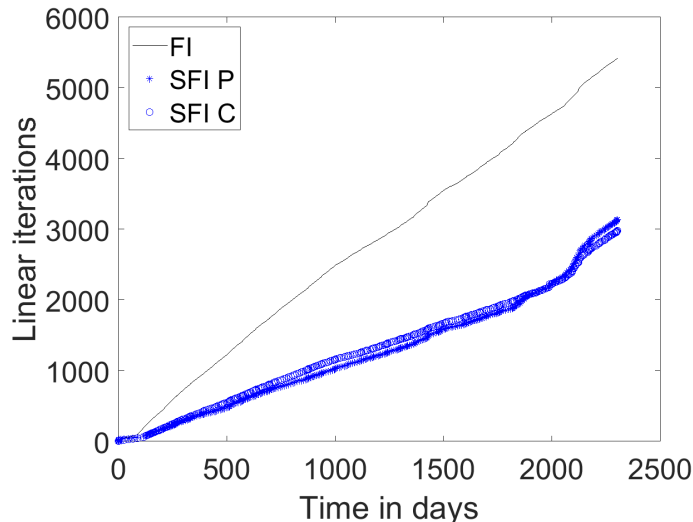


Figure 22: Cumulative CPR iterations for the FI method and cumulative linear iterations for the pressure and composition systems for the SFI method for the anticlinal model.

The compositional SFI scheme is an extended natural-variables formulation. The pressure equation used here is obtained as a weighted sum of the nonlinear component conservation equations, and it can be seen as a nonlinear overall-volume balance. This pressure equation is different from the ‘usual’ pressure equations used in sequential formulations, which are obtained as a linear combination of the linearized component conservation equations or by linear combination of the component conservation equations with constant coefficients. The nonlinear volume-balance equation simplifies to the usual volume-balance equations used by SFI methods for dead-oil and black-oil systems. There are two splitting errors associated with the compositional SFI scheme: (1) volume balance errors, and (2) total-velocity errors. Our analysis indicates that the volume-balance errors are highly localized around fronts where a phase change takes place; however, the errors in the total-velocity field can be quite large with large spatial support that spans the invaded regions of the reservoir. The total-velocity error associated with the sequential-implicit split is the primary cause of nonlinear convergence problems for SFI schemes including ours. Here, we demonstrate that the splitting errors can be reduced to arbitrarily small values when a nonlinear pressure equation is used. Moreover, we show how to effectively control the splitting errors in order to achieve convergence to any desired tolerance. We

tested the compositional SFI approach for challenging test cases in 1D, 2D and 3D. For strongly coupled problems, the SFI algorithm requires a few more iterations than the FI method, but for weakly coupled cases, the sequential algorithm requires fewer iterations than the FI method. Overall, the compositional SFI scheme enjoys convergence properties that are very competitive with the fully-implicit method, even when the coupling between the flow and the transport is quite strong. The SFI formulation has several advantages, however. With the sequential formulation, the parabolic and hyperbolic operators of compositional multi-component flow and transport are now identified and decoupled. As a result, it is now possible to design specific numerical methods optimized for each sub-problem. That includes the use of specific linear solvers for the parabolic and hyperbolic operators, as well as opening the door for advanced (high-order) spatial and temporal discretization schemes. Finally, this new SFI scheme is well suited for multi-scale compositional formulations that rely on sequential coupling of the flow and transport problems.

5. Nomenclature

- ϕ porosity of the rock
- K permeability in mD
- D depth in ft
- g gravitational acceleration in ft²-Psi/lb
- n_h number of hydrocarbon components
- MW_c molar fraction of component c
- P_p pressure of phase p in Psi
- $P_{c_{gO}}(S_g) = P_g - P_o$ capillary pressure in Psi
- $P_{c_{oW}}(S_w) = P_o - P_w$ capillary pressure in Psi
- S_p flow saturation of phase p
- S_p^{thermo} thermodynamic saturation of phase p
- \bar{S}_p^{thermo} normalized thermodynamic saturation of phase p
- x_c mole-fraction of component c in the oil phase
- y_c mole-fraction of component c in the gas phase
- z_α total mole-fraction of component $\alpha = c, w$
- β_p mole-fraction of phase p
- ρ_p phase mole density in lbmol/ft³
- ρ_t total mole density in lbmol/ft³
- $\bar{\rho}_p$ phase mass density in lb/ft³, $\bar{\rho}_g = (\sum_c y_c MW_c)\rho_g$, $\bar{\rho}_o = (\sum_c x_c MW_c)\rho_o$
and $\bar{\rho}_w = MW_w\rho_w$.
- μ_p phase dynamic viscosity in cP
- k_{r_p} relative permeability for phase p

- $\hat{f}_{c,p}$ fugacity of hydrocarbon component c in phase p in Psi
- u_p velocity of phase p in ft/day
- u_t total-velocity in ft/day
- u_t^f frozen total-velocity during the composition update in ft/day
- λ_p mobility for phase p in cP⁻¹
- λ_t total mobility in cP⁻¹
- q_p and q_t well contributions (source or sink) in lbmol/day
- R_{thermo} thermodynamic volume splitting error
- R_{u_t} normalized total-velocity splitting error
- $R_{\nabla \cdot u_t}$ normalized divergence of total-velocity splitting error
- $\overline{\nabla \cdot u_t}$ dimensionless divergence of the total-velocity
- N_α number of moles of component $\alpha = c, w$ in lbmol
- V_T total fluid volume in ft³
- V_P discretized pore volume in ft³
- Q_t total volumetric rate in ft³/day
- c_t total compressibility in Psi⁻¹
- V_{T_α} partial molar volume of component $\alpha = c, w$ in ft³/lbmol
- ξ_α density of component $\alpha = c, w$ in lbmol/ft³

6. Acknowledgments

The authors would like to thank TOTAL management for permission to publish this work and O. Møyner for constructive discussions.

7. Appendix A: Description of the Models

The 1D model used in this study has 220 cells of dimensions of $dx = 20$ ft, $dy = 10$ ft, $dz = 2$ ft. The porosity is $\phi = 0.2$ and the permeability $K = 100$ mD. The 2D model has 220×60 cells with porosity and permeabilities from the top layer of SPE 10 comparative solution project [3]. The rock compressibility for the 1D and 2D cases is $1.78e-5$ 1/Psi. The relative permeabilities are quadratic for both the oil and the gas phases. The capillary pressures are zero. The fluid is taken from the SPE 5 comparative solution project [14]. The test cases have initial conditions with $P = 4000.0$ Psi, $T = 160^\circ\text{F}$ and $S_o = 1.0$; table 3 provides the initial composition values. The connection

Table 3: Initial oil composition for SPE 5 fluid.

C_1	C_2	C_3	C_4	C_5	C_6
0.5	0.03	0.07	0.2	0.15	0.05

factors for all the cell-well connections are fixed at 0.3 Rbbl.cP/day-Psi. The fluid is produced at 1800 Psi during the depletion.

8. Appendix B: SI Metric Conversion Factors

1	Psi	=	100000/14.5037	Pa
1	ft	=	1/3.2808	m
1	lb	=	1/2.20462262	kg
1	mD	=	9.869e-16	m^2
1	cP	=	0.001	Pa.s
1	day	=	86400	s

9. References

References

- [1] G. Acs, S. Doleschall, and E. Farkas. General purpose compositional model. *Society of Petroleum Engineers Journal*, 25(04):543–553, aug 1985. doi: 10.2118/10515-pa. URL <http://dx.doi.org/10.2118/10515-PA>.
- [2] H. Cao, H.A. Tchelepi, J. Wallis, and H. Yardumian. Parallel scalable unstructured CPR-type linear solver for reservoir simulation. In *SPE*

- Annual Technical Conference and Exhibition*. Society of Petroleum Engineers (SPE), 2005. doi: 10.2118/96809-ms. URL <http://dx.doi.org/10.2118/96809-MS>.
- [3] M.A. Christie and M.J. Blunt. Tenth SPE comparative solution project: A comparison of upscaling techniques. *SPE Reservoir Evaluation & Engineering*, 4(04):308–317, aug 2001. doi: 10.2118/72469-pa. URL <http://dx.doi.org/10.2118/72469-PA>.
- [4] K.H. Coats. An equation of state compositional model. *Society of Petroleum Engineers Journal*, 20(05):363–376, oct 1980. doi: 10.2118/8284-pa. URL <http://dx.doi.org/10.2118/8284-PA>.
- [5] K.H. Coats. A note on IMPES and some IMPES-based simulation models. *SPE Journal*, 5(03):245–251, sep 2000. doi: 10.2118/65092-pa. URL <http://dx.doi.org/10.2118/65092-PA>.
- [6] K.H. Coats. IMPES stability: Selection of stable timesteps. *SPE Journal*, 8(02):181–187, jun 2003. doi: 10.2118/84924-pa. URL <http://dx.doi.org/10.2118/84924-PA>.
- [7] R.B. Crookston, W.E. Culham, and W.H. Chen. A numerical simulation model for thermal recovery processes. *Society of Petroleum Engineers Journal*, 19(01):37–58, feb 1979. doi: 10.2118/6724-pa. URL <http://dx.doi.org/10.2118/6724-PA>.
- [8] E.M. Dicks. *Higher Order Godunov Black-Oil Simulations for Compressible Flow in Porous Media*. PhD thesis, University of Reading, Department of Mathematics, March 1993.
- [9] F. Doster, E. Keilegavlen, and J.M. Nordbotten. *A robust implicit pressure explicit mass method for multi-phase multi-component flow including capillary pressure and buoyancy*. CRC Press, apr 2014. doi: doi:10.1201/b16790-11. URL <https://doi.org/10.1201/b16790-11>.
- [10] B. Faigle, M.A. Elfeel, R. Helmig, B. Becker, B. Flemisch, and S. Geiger. Multi-physics modeling of non-isothermal compositional flow on adaptive grids. *Computer Methods in Applied Mechanics and Engineering*, 292(Supplement C):16 – 34, 2015. ISSN 0045-7825. doi: <https://doi.org/10.1016/j.cma.2014.11.030>. URL <http://www.sciencedirect.com/science/article/pii/S0045782514004630>.

- [11] H. Hajibeygi and H.A. Tchelepi. Compositional multiscale finite-volume formulation. *SPE Journal*, 19(02):316–326, apr 2014. doi: 10.2118/163664-pa. URL <http://dx.doi.org/10.2118/163664-PA>.
- [12] P. Jenny, S.H. Lee, and H.A. Tchelepi. Adaptive fully implicit multi-scale finite-volume method for multi-phase flow and transport in heterogeneous porous media. *Journal of Computational Physics*, 217(2): 627 – 641, 2006. ISSN 0021-9991. doi: <http://dx.doi.org/10.1016/j.jcp.2006.01.028>. URL <http://www.sciencedirect.com/science/article/pii/S002199910600026X>.
- [13] M. Khait and D.V. Voskov. Operator-based linearization for general purpose reservoir simulation. *Journal of Petroleum Science and Engineering*, 157:990 – 998, 2017. ISSN 0920-4105. doi: <https://doi.org/10.1016/j.petrol.2017.08.009>. URL <http://www.sciencedirect.com/science/article/pii/S0920410516310907>.
- [14] J. E. Killough and C. A. Kossack. Fifth comparative solution project: Evaluation of miscible flood simulators. In *SPE Symposium on Reservoir Simulation*. Society of Petroleum Engineers (SPE), 1987. doi: 10.2118/16000-ms. URL <http://dx.doi.org/10.2118/16000-MS>.
- [15] S.H. Lee, C. Wolfsteiner, and H.A. Tchelepi. Multiscale finite-volume formulation for multiphase flow in porous media: black oil formulation of compressible, three-phase flow with gravity. *Computational Geosciences*, 12(3):351–366, 2008. ISSN 1420-0597. doi: 10.1007/s10596-007-9069-3. URL <http://dx.doi.org/10.1007/s10596-007-9069-3>.
- [16] J.J. Martin. Cubic equations of state-which? *Industrial & Engineering Chemistry Fundamentals*, 18(2):81–97, may 1979. doi: 10.1021/i160070a001. URL <http://dx.doi.org/10.1021/i160070a001>.
- [17] M.L. Michelsen and J. Mollerup. *Thermodynamic Models: Fundamentals and Computational Aspects, Second edition*. Tie-Line Publications, 2007.
- [18] A. Moncorgé, H. Tchelepi, and P. Jenny. New sequential scheme for mixed-implicit compositional flow simulation. In *15th European Conference on the Mathematics of Oil Recovery 2016 (ECMOR XV)*. European Association of Geoscientists & Engineers (EAGE), aug 2016.

- doi: 10.3997/2214-4609.201601895. URL <http://dx.doi.org/10.3997/2214-4609.201601895>.
- [19] A. Moncorgé, P. Jenny, and H.A. Tchelepi. Stable sequential fully implicit scheme for compositional simulation. In *SIAM Conference on Mathematical and Computational Issues in the Geosciences*. Society of Industrial and Applied Mathematics (SIAM), sep 2017. URL <http://www.siam-gs17.de>.
- [20] A. Moncorgé, H.A. Tchelepi, and P. Jenny. Modified sequential fully implicit scheme for compositional flow simulation. *Journal of Computational Physics*, 337:98 – 115, 2017. ISSN 0021-9991. doi: <https://doi.org/10.1016/j.jcp.2017.02.032>. URL <http://www.sciencedirect.com/science/article/pii/S0021999117301250>.
- [21] O. Møyner. A multiscale restriction-smoothed basis method for high contrast porous media represented on unstructured grids. In *Workshop on Multiphysics, Multiscale, and Coupled Problems in Subsurface Physics*. Institute for Pure & Applied Mathematics, An NSF Math Institute at UCLA, apr 2017. URL <http://www.ipam.ucla.edu>.
- [22] O. Møyner and K.-A. Lie. A multiscale restriction-smoothed basis method for compressible black-oil models. *SPE Journal*, 21(06):2079–2096, dec 2016. doi: 10.2118/173265-PA. URL <http://dx.doi.org/10.2118/173265-PA>.
- [23] O. Møyner and H. Tchelepi. Comparison of splitting schemes for compositional multiscale solvers. In *SIAM Conference on Mathematical and Computational Issues in the Geosciences*. Society of Industrial and Applied Mathematics (SIAM), sep 2017. URL <http://www.siam-gs17.de>.
- [24] O. Møyner and H.A. Tchelepi. A multiscale restriction-smoothed basis method for compositional models. In *SPE Reservoir Simulation Conference 2017*. Society of Petroleum Engineers (SPE), feb 2017. doi: 10.2118/182679-MS. URL <https://doi.org/10.2118/182679-MS>.
- [25] ResInsight Post Processing of Reservoir Simulations. The Open Porous Media Initiative, Norway, 2017. URL <http://opm-project.org>.
- [26] G.S.H. Pau, J.B. Bell, A.S. Almgren, K.M. Fagnan, and M.J. Lijewski. An adaptive mesh refinement algorithm for compressible two-phase flow

- in porous media. *Computational Geosciences*, 16(3):577–592, Jun 2012. ISSN 1573-1499. doi: 10.1007/s10596-011-9270-2. URL <http://dx.doi.org/10.1007/s10596-011-9270-2>.
- [27] D.-Y. Peng and D.B. Robinson. A new two-constant equation of state. *Industrial & Engineering Chemistry Fundamentals*, 15(1):59–64, feb 1976. doi: 10.1021/i160057a011. URL <http://dx.doi.org/10.1021/i160057a011>.
- [28] O. Redlich and J. N. S. Kwong. On the Thermodynamics of Solutions. V. An Equation of State. Fugacities of Gaseous Solutions. *Chemical Reviews*, 44(1):233–244, feb 1949. doi: 10.1021/cr60137a013. URL <http://dx.doi.org/10.1021/cr60137a013>.
- [29] G. Soave. Equilibrium constants from a modified Redlich-Kwong equation of state. *Chemical Engineering Science*, 27(6):1197–1203, jun 1972. doi: 10.1016/0009-2509(72)80096-4. URL [http://dx.doi.org/10.1016/0009-2509\(72\)80096-4](http://dx.doi.org/10.1016/0009-2509(72)80096-4).
- [30] J.A. Trangenstein and J.B. Bell. Mathematical structure of the black-oil model for petroleum reservoir simulation. *SIAM Journal on Applied Mathematics*, 49(3):749–783, 1989. doi: 10.1137/0149044. URL <https://doi.org/10.1137/0149044>.
- [31] J.A. Trangenstein and J.B. Bell. Mathematical structure of compositional reservoir simulation. *SIAM Journal on Scientific and Statistical Computing*, 10(5):817–845, 1989. doi: 10.1137/0910049. URL <https://doi.org/10.1137/0910049>.
- [32] D.V. Voskov and H.A. Tchelepi. Compositional space parameterization: Multicontact miscible displacements and extension to multiple phases. *Society of Petroleum Engineers Journal*, 14(03), sep 2009. doi: 10.2118/113492-PA. URL <http://dx.doi.org/10.2118/113492-PA>.
- [33] J.W. Watts. A compositional formulation of the pressure and saturation equations. *SPE Reservoir Engineering*, 1(03):243–252, may 1986. doi: 10.2118/12244-pa. URL <http://dx.doi.org/10.2118/12244-PA>.
- [34] L.C. Young. Continuous compositional volume-balance equations. In *SPE Symposium on Reservoir Simulation*. Society of Petroleum Engi-

neers (SPE), 2001. doi: 10.2118/66346-MS. URL <https://doi.org/10.2118/66346-MS>.

- [35] R. Zaydullin, D. Voskov, and H.A. Tchelepi. Nonlinear formulation based on an equation-of-state free method for compositional flow simulation. *Society of Petroleum Engineers Journal*, 18(02), dec 2012. doi: 10.2118/146989-PA. URL <https://doi.org/10.2118/146989-PA>.